SEG Special Publications, no. 24, pp. 49–68

Chapter 4

Timing and Nature of Mineralization and Associated Hydrothermal Alteration at the Öksüt High-Sulfidation Epithermal Au-Cu Deposit (Kayseri Province, Central Anatolia)

Emrecan Yurdakul,[1,2] Ali İmer,[2,†] and Mustafa Cihan[1]

[1]*Centerra Madencilik A.Ş. (Centerra Gold Inc.), Ankara, Turkey*

[2]*Department of Geological Engineering, Middle East Technical University, Ankara 06800, Turkey*

Abstract

Öksüt is a breccia-hosted high-sulfidation epithermal gold-copper deposit, situated within the Develidağ Volcanic Complex in south-central Anatolia. The volcanic complex, exposed on the northern edge of the Tauride range, is largely made up of late Miocene andesitic to dacitic porphyries, covered by a succession of Pliocene basalts and basaltic andesites. A series of N-S- to NNW-trending faults of the regional central Anatolian fault zone partly cut and border the volcanic complex to the east and west.

Mineralization at Öksüt follows a predominant north-northwest trend that correlates well with the regional stress regime. The bulk of the mineralization occurs in two domains, the Keltepe and Güneytepe orebodies, where steeply dipping and pervasively supergene oxidized breccia zones exploited funnel-shaped diatreme conduits within pyroxene andesite porphyry. Emplacement of these phreatomagmatic breccias was largely controlled by vertical to subvertical faults with dominant normal-slip components.

Mineralized breccias comprise a central zone of residual vuggy to massive silica alteration, laterally and vertically grading into zones of quartz-alunite and quartz-alunite-clay alteration. These silica-altered breccias contain relatively high gold grades, whereas significant mineralization was also encountered in quartz-alunite-clay alteration. In the oxide zone, gold occurs in native form, whereas in the hypogene zone it occurs both as native gold or within pyrite-enargite accompanied by marcasite, and rare chalcopyrite and tetrahedrite. To the west of Keltepe and in Güneytepe, at depth, the altered and mineralized breccias pass into barren zones of argillic and then into biotite-magnetite ± K-feldspar ± anhdyrite alteration, the latter typical of porphyry-type systems. Sporadic zones of calc-silicate alteration, represented by grossularite, diopside, and vesuvianite, are also present.

Three $^{40}Ar/^{39}Ar$ ages obtained from alunite and illite range between 5.7 to 5.5 Ma and are concordant with previously reported U-Pb and $^{40}Ar/^{39}Ar$ ages (~6–5.5 Ma) from host pyroxene andesite porphyry. This suggests that high-sulfidation alteration and mineralization developed contemporaneously with postsubduction magmatism at the Develidağ Volcanic Complex, in relationship to regional E-W-directed extension that commenced at ~6 Ma. Our new ages also confirm Öksüt as the youngest epithermal gold deposit discovered to date in Anatolia, and possibly in the entire Western Tethyan metallogenic belt.

The topographic prominence of the volcanic edifice combined with high permeability of the breccias favored deep supergene sulfide oxidation, thereby rendering Öksüt economically viable. Gold encapsulated in hypogene sulfides was liberated during the oxidation, whereas the copper was leached to produce a discontinuous chalcocite- and covellite-dominated enrichment zone, up to 50 m thick, at the base of oxidation.

Introduction

The collided Tethyan margins of Anatolia are characterized by widespread volcano-plutonic complexes of Late Cretaceous to late Cenozoic age. These magmatic systems are responsible for formation of much of the metallic ore deposits inventory of Turkey. In particular, the middle Eocene to Miocene volcanic complexes are fairly well preserved and host numerous small- to large-sized epithermal systems (Yiğit, 2012; Kuşcu et al., 2019; Rabayrol et al., 2019). Most of these deposits, including significant examples such as Çöpler, Efemçukuru, and Ovacık, are restricted to a few mineral belts such as the Biga Peninsula, western Anatolia, eastern Taurides, and eastern Pontides (Fig. 1).

In striking contrast to the aforementioned mineral belts, central Anatolia received less exploration despite widespread postcollisional and, therefore, potentially prospective volcanism (Fig. 1). Late Cenozoic volcanic sequences exposed in south-central Anatolia were historically the focus of small-scale gold, silver, mercury, and antimony mining (Akçay, 1995; Yiğit, 2009), but apart from these no significant base and/or precious metal mineralization was discovered prior to the mid-2000s. Increased exploration efforts during the past two decades revealed an important potential in this volcanic belt, particularly for epithermal Au and porphyry Cu ± Mo ± Au mineralization. Consequently, three gold mines (Öksüt, İnlice, and Himmetdede; Fig. 1) were recently entered into production. In addition, several other prospects, mainly clustered in the Konya (e.g., Doğanbey porphyry Cu-Mo-Au and Karacaören porphyry Au) and Melendiz (e.g., Tepeköy epithermal

†Corresponding author: e-mail address, aimer@metu.edu.tr

Open Access (CC-BY-NC) publication of the Jeremy P. Richards memorial volume was generously supported by BHP Metals Exploration and the Laurentian University Mineral Exploration Research Centre (MERC) and Harquail School of Earth Sciences (HES).

Digital Appendices are available online at www.segweb.org/SP24-Appendices.
doi: 10.5382/SP.24.04; 20 p.

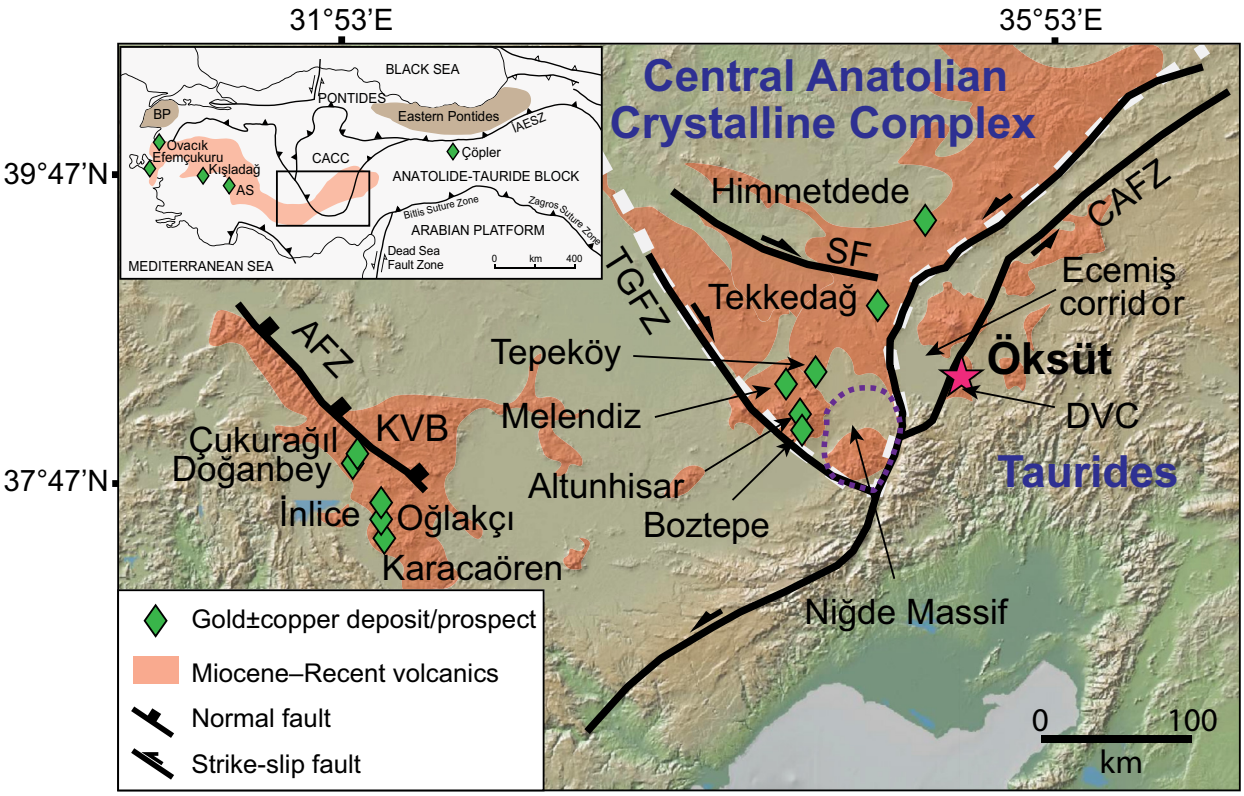

Fig. 1. Regional map showing distribution of late Cenozoic to Recent volcanic rocks and major structural elements of south Anatolia (after Koçyiğit and Beyhan, 1998; Koçyiğit and Erol, 2001; MTA, 2002). Regionally important porphyry and epithermal occurrences are also shown. Digital elevation map retrieved from GeoMap App (https://geomapapp.org). Inset map shows the major tectonic terranes of Turkey, major mineral belts, late Cenozoic central and western Anatolian volcanic belt, and gold ± copper deposits cited in the text. Box in the inset indicates the extent of the main map. Abbreviations: AFZ = Akşehir fault zone, BP = Biga Peninsula, CAFZ = central Anatolian fault zone, DVC = Develidağ Volcanic Complex, IAESZ = Izmir-Ankara-Erzincan suture zone, KVB = Konya volcanic belt, SF = Salanda fault.

Au) volcanic fields (Fig. 1), were also identified in close spatial relationship to stratovolcanoes and monogenetic lava domes (Yıldız, 2013). Published ages from and nearby these mineralized centers indicated that associated magmatism occurred between 14 and 3 Ma (e.g., Innocenti et al., 1975; Besang et al., 1977; Aydar et al., 2012; Kuşcu et al., 2019; Rabayrol et al., 2019), including ~6 to 5.5 Ma zircon U-Pb ages from the Develidağ volcanics hosting the Öksüt deposit (Rabayrol et al., 2019; Aluç et al., 2020). Nevertheless, the temporal relationship between volcanism and epithermal-style alteration and mineralization at Öksüt as well as in these other districts was unknown.

Öksüt is currently the most significant gold system in central Turkey. Bulk mineable gold occurs in two principal sectors, the Keltepe and Güneytepe deposits. Öksüt has total proven and probable reserves of 1.27 Moz Au, and additional measured and indicated resources of 0.21 Moz Au (Centerra Gold: https://www.centerragold.com/operations/oksut/resource-estimate; accessed 30 August 2020). Bulk of this is hosted in Keltepe, whereas the Güneytepe orebody in the south is a much smaller resource. Several satellite prospects, including Yelibelen, Keltepe NW, and Büyüktepe, were also highlighted subsequently, and these are currently being drill tested. In this study, we report on the geology and geochronology, as well as on alteration and mineralization characteristics of the Öksüt district, and aim to highlight the regional metallogenic significance of this youngest (based on this study) member of the postsubduction family of deposits in Anatolia. Presented geologic information builds on previous work by Yıldız et al. (2016, 2017) and is based on detailed field mapping, whereas observations on alteration and mineralization are based on detailed petrographic and mineralogic analyses of drill core samples from the Keltepe and Güneytepe orebodies.

Exploration History

Öksüt was initially discovered in 2007 by Stratex International plc. during reconnaissance exploration of the late Cenozoic volcanic belt across south-central Anatolia (Fig. 1). The initial discovery was based on recognition of numerous silicified ledges scattered within the andesitic volcanic rocks of the Develidağ Volcanic Complex (Yıldız et al., 2016, 2017; Figs. 1, 2). Surface samples from and nearby the silicified ledges (Fig. 3A) returned significantly high gold grades, and follow-up drilling of highlighted targets confirmed gold-copper mineralization largely hosted within steeply dipping breccia bodies (Yıldız et al., 2017). In 2009, Stratex established a joint venture with Centerra Gold and continued an extensive district-wide drilling program. Centerra Gold fully acquired the property in December 2012 and began gold production from

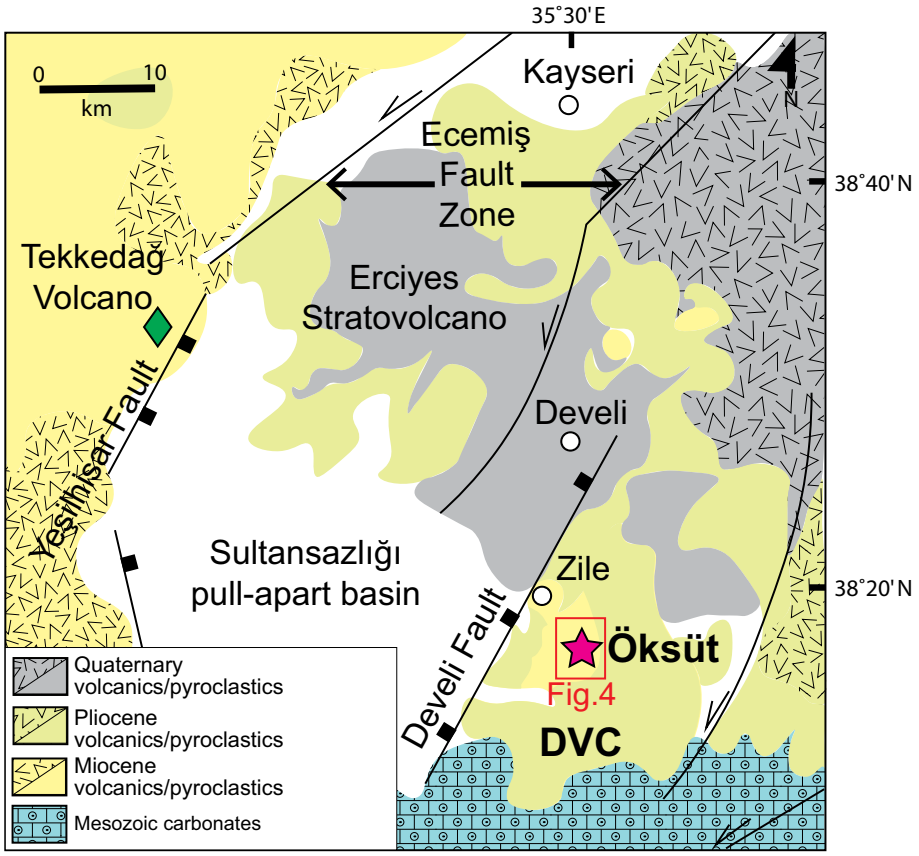

Fig. 2. Simplified geologic map of the Ecemiş corridor (modified from MTA, 2002).

both the Keltepe and Güneytepe pits in early 2020, with an expected mine life of eight years (Cihan et al., 2016).

Geologic Setting

The Öksüt deposit is located in the Develi district, approximately 45 km south of Kayseri in central Anatolia (Figs. 1, 2). Gold-copper mineralization at Öksüt is hosted by the late Miocene-Pliocene Develidağ Volcanic Complex, which was emplaced along the Ecemiş sector of the central Anatolian fault zone, a prominent sinistral transcurrent fault zone (Figs. 1, 2; Koçyiğit and Beyhan, 1998). The Ecemiş fault zone, separating the central Anatolian Crystalline Complex from the Tauride platform (Figs. 1, 2), was initiated during the Late Cretaceous-Paleogene and later reactivated episodically particularly during the Miocene to Recent times (Koçyiğit and Beyhan, 1998; Jaffey and Robertson, 2001). The Ecemiş fault zone accommodated part of the compression induced by mid-Miocene Afro-Arabia–Eurasia collision (Jaffey and Robertson, 2001) and also exercised a strong control on localization of Neogene volcanic activity in south-central Anatolia (Innocenti et al., 1975; Pasquare et al., 1988).

Late Cenozoic volcanism in south-central Anatolia developed following early to middle Miocene closure of the Southern Neotethys Basin (20–12 Ma), and collision and suturing of the Tauride-Anatolide block and the Arabian terranes in Central and eastern Anatolia (Robertson et al., 2007; Okay et al., 2010). Volcanic activity was initiated during the late Miocene (~11 Ma), shortly after a decrease in Africa-Eurasia convergence rate and consequent switch from compression to extension/transtension (Delph et al., 2017). This magmatic phase continued well into recent times almost uninterrupted except for short pulses of quiescence, with main peaks recorded at ~9 to 8 and ~7 to 5 Ma (Aydar et al., 2012). From 8 Ma onward, the south margin of central Anatolia and juxtaposed Tauride range have undergone >2 km of uplift (Schildgen et al., 2012), which was proposed to have resulted from westward propagation of slab detachment that had already started in eastern Anatolia in the early to middle Miocene, and attendant mantle upwelling (Cosentino et al., 2012; Schildgen et al., 2012).

Late Miocene to Recent postsubduction volcanism in south-central Anatolia is attributed to foundering of mantle lithosphere beneath central Anatolia (Bartol and Govers, 2014; Delph et al., 2017; Göğüş et al., 2017), which culminated in production of widespread ignimbrite deposits as well as numerous stratovolcanoes, monogenetic lava flows, dome complexes, and cone clusters (Innocenti et al., 1975; Pasquare et al., 1988). Volcanic products display varying compositions from basalt through andesite-dacite to rhyolite, which are predominantly calc-alkaline to mildly alkaline and show arc-like affinities (e.g., Gencalioglu-Kuscu and Geneli, 2010; Kürkcüoglu, 2010; Reid et al., 2017), indicating a significant contribution from previous subduction-modified mantle lithosphere.

The Develidağ Volcanic Complex lies immediately to the east of the main axis of the Ecemiş fault zone, where it

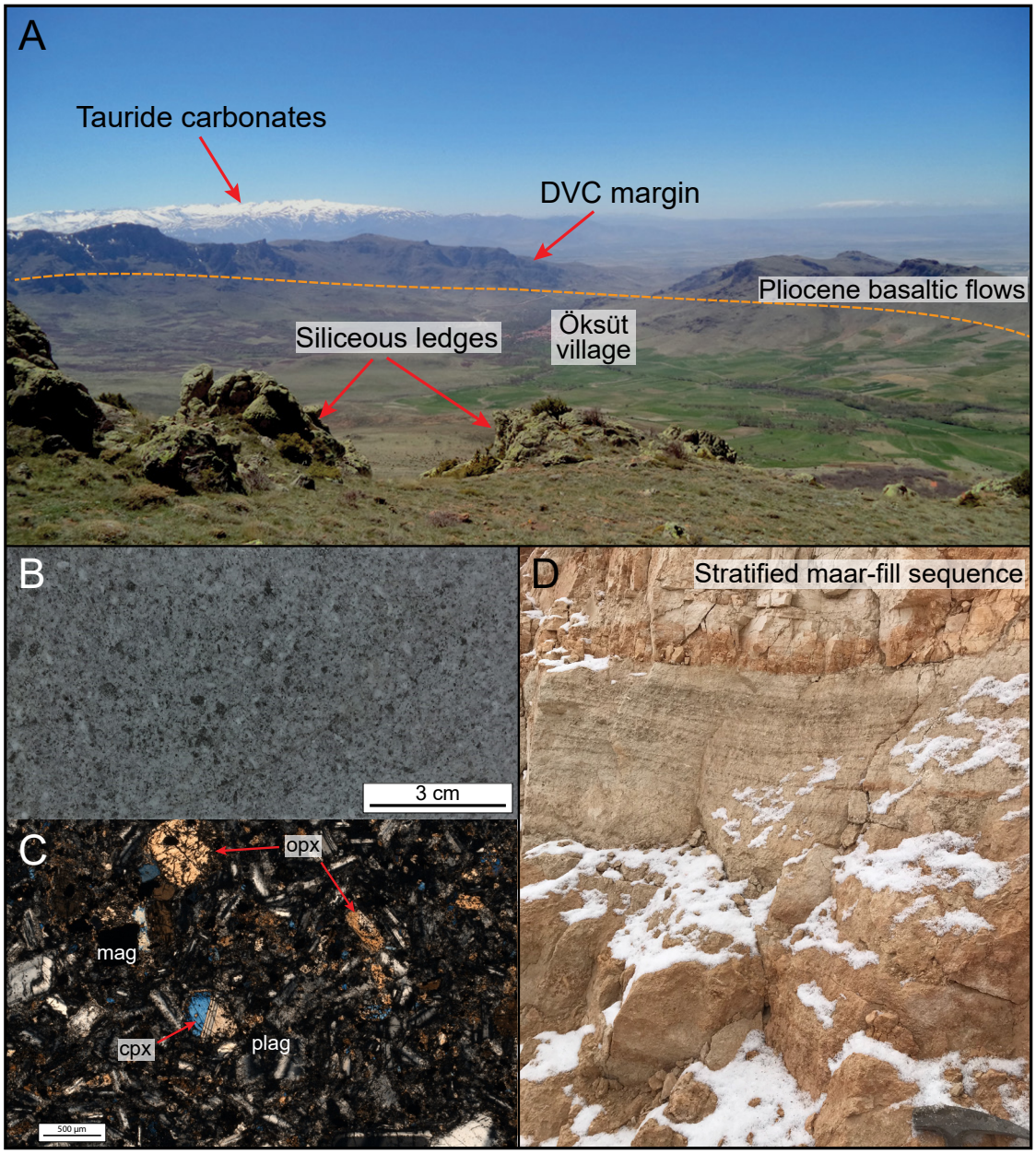

Fig. 3. Photographs of the Develidağ Volcanic Complex (DVC) and major lithologies in Öksüt. A. View from Öksüt deposit toward the southern sector of the Complex marked by Pliocene basaltic flows. Mineralized siliceous ledges remain as resistant topographic features in the foreground. Taurus platform carbonates are exposed in the mountain terrane in the background. Drill core (B) and photomicrograph (C) of the least altered pyroxene andesite porphyry. D. Thinly bedded maar-fill deposits exposed in the western wall of Keltepe pit. Abbreviations: cpx = clinopyroxene, mag = magnetite, opx = orthopyroxene, plag = plagioclase.

borders the Sultansazlığı pull-apart basin (Figs. 1, 2). Based on previously published $^{40}Ar/^{39}Ar$ and LA-ICP-MS U-Pb zircon age data, emplacement of the Develidağ Volcanic Complex occurred during the latest Miocene (~6.3–5.4 Ma; Jaffey et al., 2004; Rabayrol et al., 2019; Aluç et al., 2020), coincident with the onset of east-west extension and associated normal faulting along the Ecemiş fault zone (Toprak and Göncüoğlu, 1993; Koçyiğit and Beyhan, 1998; Jaffey et al., 2004).

The Develidağ Volcanic Complex was partly collapsed and faulted down on the western flank for at least 300 m along the Develi fault, against the Plio-Quaternary volcanic infill of the Sultansazlığı pull-apart basin (Fig. 2; Koçyiğit and Erol, 2001). The remaining part of the complex overlies the Permo-Carboniferous metacarbonates of the Tauride range and is dominated by Miocene-Pliocene volcanic and volcaniclastic lithologies with a surface extent of >300 km² (Fig. 2). Thin sheets of ignimbrites regionally surround the lavas of the complex to the north and south.

In the immediate deposit area, most of the volcanic units have undergone extensive hydrothermal alteration, and therefore the original host rock is often difficult to distinguish in the shallow epithermal levels. The lower part of the volcanic

stratigraphy comprises at least two distinct late Miocene andesitic to dacitic porphyries, which collectively represent a dome complex. The first of these is a hornblende-phyric dacite porphyry, which was encountered outside the main core of the mineralized system. This unit consists of phenocrystic hornblende and plagioclase set in a fine-grained to glassy matrix and shows minor alteration to clay minerals. Aluç et al. (2020) reported U-Pb zircon ages of 5.78 ± 0.01 and 5.73 ± 0.06 Ma from dacite porphyry, whereas $^{40}Ar/^{39}Ar$ fusion (plagioclase) ages of 6.29 ± 0.07 and 5.80 ± 0.11 Ma were obtained from the exposures near Zile (Fig. 2; Jaffey et al., 2004).

Pyroxene andesite porphyry is the main wall rock to the gold-copper mineralization (Fig. 3B-C). This unit has a phenocryst assemblage of clinopyroxene and plagioclase with minor orthopyroxene and sparse biotite embedded in a groundmass containing plagioclase and magnetite microphenocrysts (Fig. 3C). In deeper drill holes to the west of the Keltepe pit (ODD-337; Fig. 4), pyroxene andesite porphyry was encountered to depths of >700 m. Three samples of pyroxene andesite porphyry yielded U-Pb zircon ages of 5.70 ± 0.02, 5.67 ± 0.07, and 5.36 ± 0.02 Ma (Rabayrol et al., 2019; Aluç et al., 2020), indicating overlapping or slightly younger timing for this unit compared to dacite porphyry.

A partly concealed, funnel-shaped diatreme structure also exists along the western wall of the Keltepe pit, capped by ~10-m-thick maar-fill deposits consisting of thinly bedded volcaniclastics (Fig. 3D). Similar stratified but intensely silica-replaced intervals were also encountered in nearby drill holes from the Keltepe pit.

Pliocene basalt-basaltic andesite flow-banded lavas form the younger volcanic cover throughout the eastern part of the volcanic complex at higher elevations (Fig. 4; Kürkcüoglu, 2010) and also occur along the margins of the Develidağ Volcanic Complex (Fig. 3A). These are distinguished from massive andesite to dacite porphyries by their gently outward-dipping flow banding. This unit is neither altered nor mineralized and is characterized by olivine, pyroxene, and plagioclase both as phenocryst and as groundmass phases, alongside minor amounts of magnetite microphenocrysts. Dikes and sills of similar composition were also observed in drill core crosscutting the pyroxene andesite porphyry, and these were considered as feeders to shallower basaltic lavas.

The Develidağ Volcanic Complex is cut by NNE-, NE-, and NW-trending, steeply dipping oblique faults that can be traced over several hundred meters along strike (Fig. 4). NNE-trending faults mainly display sinistral movement, whereas NE- and NW-trending faults are predominantly normal-slip with a minor strike-slip component. The structural blocks bounded by this latter group of faults have systematically stepped down to the southwest. Intermittent seismic activity of the Ecemiş fault zone since the Miocene (Koçyiğit and Beyhan, 1998) resulted in widespread postmineralization fault reactivation, and therefore it is difficult to resolve relative timing of different fault populations at Öksüt unequivocally. Nevertheless, both NW- and NNE-trending faults were consistently observed as crosscut by the NE-trending faults (Cihan et al., 2016). On the other hand, all three fault populations seem to have exerted structural control on localization and emplacement of subvertical breccia bodies and associated hydrothermal alteration (Fig. 5A). Silica ledges, in particular, developed at intersections of NW- and NE-trending faults. The latter host much of the gold mineralization at Güneytepe (Fig. 4).

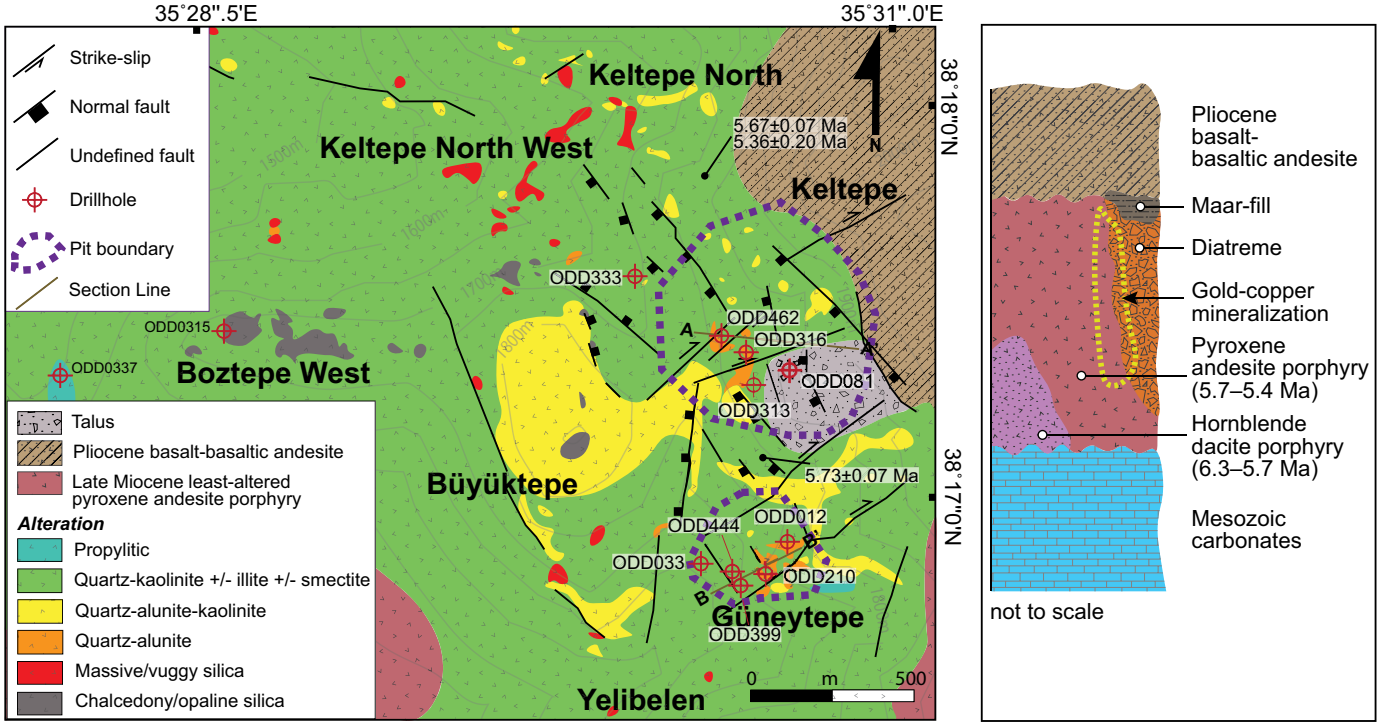

Fig. 4. Detailed surface geology, alteration map (modified after Yıldız et al., 2017), and representative columnar section of Öksüt. Locations of Keltepe and Güneytepe pits as well as of key drill holes cited in the text are also shown. Ages shown in columnar section are from Jaffey et al. (2004), Rabayrol et al. (2019), and Aluç et al. (2020).

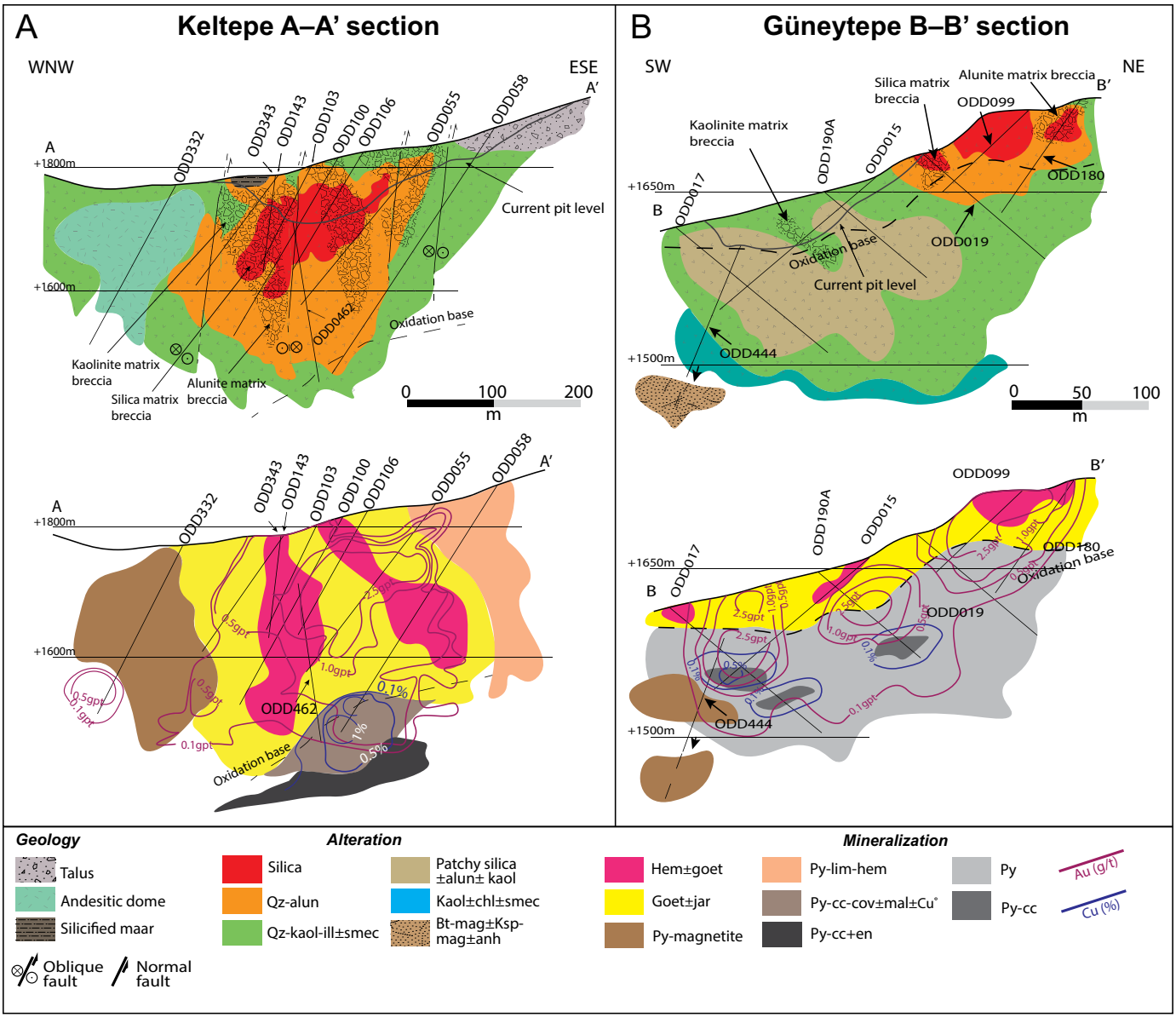

Fig. 5. Schematic cross sections of (A) Keltepe and (B) Güneytepe orebodies, showing spatial relationship between various alteration and mineralization domains as well as gold-copper grade shells. Section lines are shown in Figure 4. Abbreviations: alun = alunite, anh = anhydrite, bt = biotite, cc = chalcocite, chl = chlorite, cov = covellite, en = enargite, goet = goethite, hem = hematite, ill = illite, kaol = kaolinite, Ksp = K-feldspar, lim = limonite, mag = magnetite, py = pyrite, qz = quartz, smec = smectite.

The NW-trending faults also mark the contact between pyroxene andesite porphyry and Pliocene basaltic flows, now largely concealed underneath the landslide material of Pliocene basaltic lava flows cover at the southeast border of the Keltepe pit (Fig. 4). All three fault generations extend into this talus material as well as into the basaltic cover units (Fig. 4), suggesting postmineralization fault reactivation. This is also supported by sulfide slickensides observed in drill core with dextral oblique-slip movement.

Deposit Characteristics

Gold-copper mineralization and associated hydrothermal alteration at Öksüt is generally confined to steeply dipping breccia bodies also referred to as "ledges" (Figs. 5, 6; Yıldız et al., 2016). Two main mineralized domains were identified by Yıldız et al. (2016, 2017), the Keltepe and Güneytepe orebodies, located about 400 m apart in the north-south direction (Fig. 4). Keltepe and Güneytepe display broadly similar alteration and mineralization styles as well as overall gangue and ore mineralogy, primarily developed within structurally controlled upward-flaring breccia zones (Figs. 5, 6). Figure 7 provides the paragenetic sequence of ore and alteration minerals as established from pit and drill core observations from both orebodies.

Hydrothermal alteration

Silicic alteration: Silicic alteration represents the earliest phase of shallow epithermal alteration and defines the core

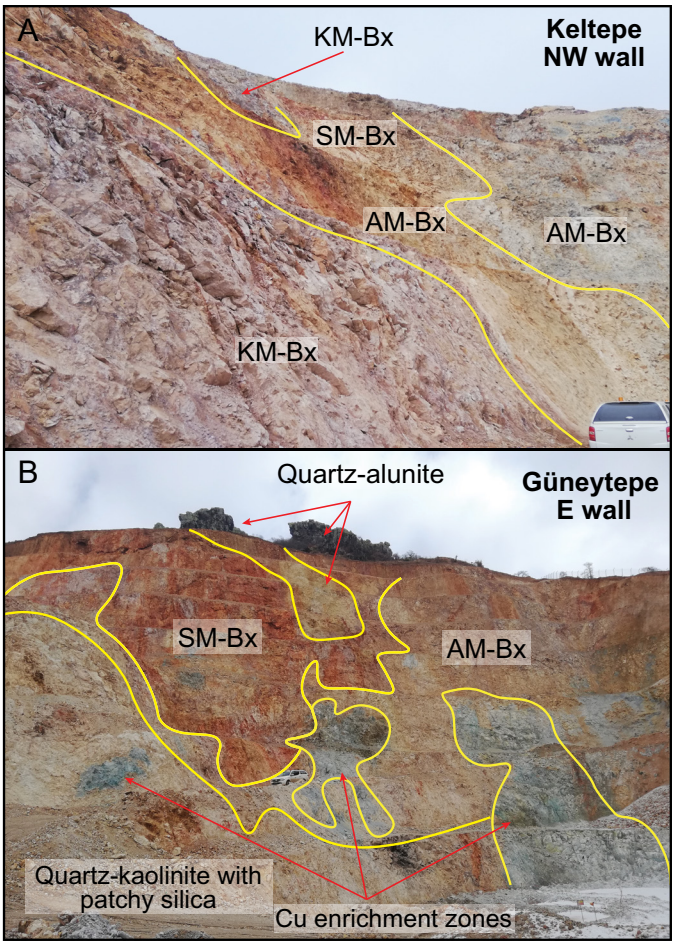

Fig. 6. Distribution of altered and mineralized domains, as well as various breccia facies in (A) Keltepe and (B) Güneytepe pits. Abbreviations: AM-Bx = alunite-matrix breccia, KM-Bx = kaolinite-matrix breccia, SM-Bx = silica-matrix breccia.

of the mineralized breccias (Figs. 5, 6). It is characterized by complete replacement of the original volcanic lithologies and comprises variably textured zones of residual vuggy (Fig. 8A) and massive silica. Within zones of silicic alteration, fine-grained quartz has replaced breccia clasts and matrix material (Fig. 8B) as well as andesite porphyry. In the upper 10 to 20 m of the silicic zones, however, opaline silica and porcellaneous chalcedony, rather than fine-grained quartz, are present likely due to lower temperatures. More sugary varieties of quartz are also observed in both Keltepe and Güneytepe.

In Keltepe, at the surface, zones of silicic alteration are generally restricted to the north of the pit area (Figs. 4, 5A, 6A), where they form resistant ledges that can be traced for >100 m. They are, however, more extensive in deeper parts within the pit area and in Güneytepe (Figs. 4, 5B, 6B).

Quartz-alunite ± kaolinite alteration: Quartz-alunite ± kaolinite alteration is most commonly observed in, but not restricted to, breccia bodies as an envelope to the silicic cores (Figs. 5, 6). It is vertically extensive, locally having developed at depths of >400 m west of Keltepe (Fig. 6) and shows a marked spatial zonation. An inner zone of quartz-alunite passes outward into an assemblage of quartz-kaolinite ± alunite (Figs. 5A, 6) with minor pyrophyllite and dickite (as confirmed by XRD) with or without native sulfur and diaspore. However, such zonation is not apparent along vertical profiles and downward transition between the two assemblages is not systematic. Extensive zones of quartz-alunite ± kaolinite alteration were mapped to the west of the Keltepe pit and in between the Keltepe and Güneytepe orebodies (Fig. 4).

Distinct varieties of hypogene, white to creamy white and pinkish alunite (both as K-alunite and natro-alunite) were identified in the quartz-alunite ± kaolinite alteration zone. Fine-grained early-stage alunite replaced groundmass or phenocryst phases in andesite porphyry (Fig. 8C), and in both breccia clasts and matrix. Altered rocks of this stage are usually barren. Medium- to coarse-grained tabular prismatic to needle-like alunite (Fig. 8D) is later in the paragenesis and occurs either in groundmass or as vug infill (Fig. 8D), commonly together with Fe and Cu sulfides, and gold. Hypogene alunite also occurs as vein infill along hairline fractures, commonly at deeper levels of the quartz-alunite ± kaolinite alteration.

Quartz-alunite and quartz-kaolinite zones locally contain patches of silica characterized by irregular masses of fine-grained quartz surrounded by kaolinite and locally alunite (Fig. 8E). This distinct variety of quartz-alunite ± kaolinite alteration is more widely developed at Güneytepe, both in shallow levels and also at depth (Yıldız et al., 2017). In Keltepe, patchy silica zones are restricted to deeper levels around 300 m. Quartz-alunite ± kaolinite-altered rocks at Öksüt generally yield gold grades of >0.5 g/t.

Illite-kaolinite alteration: Illite-kaolinite alteration is the most widespread form of hydrothermal alteration in Öksüt at and near the surface (Fig. 4). It flanks and underlies zones of quartz-alunite ± kaolinite alteration and marks the lower limit of the breccia bodies at depths of >350 m (Fig. 5), representing the transition from shallow epithermal alteration to deeper high-temperature biotite-magnetite ± K-feldspar ± anhdyrite alteration.

In contrast to zones of silicic and quartz-alunite ± kaolinite alteration, primary igneous textures in zones of illite-kaolinite alteration are generally well-preserved (Fig. 8F). Illite and kaolinite are the predominant phyllosilicate phases (Fig. 8F-G) and occur together with fine-grained quartz, and minor smectite, pyrite, marcasite, and rutile. Rocks showing this alteration are typically gray to beige colored in drill core and are often crosscut by stockwork veinlets of Fe sulfides, illite, and kaolinite with or without quartz (Fig. 8G). No gold mineralization is associated with this alteration style.

Biotite-magnetite ± K-feldspar ± anhydrite alteration: Biotite-magnetite ± K-feldspar ± anhdyrite alteration (Fig. 8H-I), resembling those commonly observed in potassically altered cores of porphyry deposits (Sillitoe, 2010), is restricted to deeper levels (starting from ~350 to >700 m) in the west of Keltepe and underneath the Güneytepe pit (Yıldız et al., 2017; Fig. 5B). Fine-grained, anhedral secondary biotite dominates the altered rocks and occurs as aggregates at sites of pyroxene phenocrysts (Fig. 8I). Magnetite is typically present as disseminations and less commonly as hairline M veinlets (sensu Arancibia and Clark, 1996; Fig. 8H-I), whereas minor K-feldspar developed after plagioclase. Anhydrite was locally observed as groundmass replacements. Quartz veining, characteristic of porphyry systems (e.g., A- or B-type veins), is absent in the altered rocks. Similarly, this alteration zone

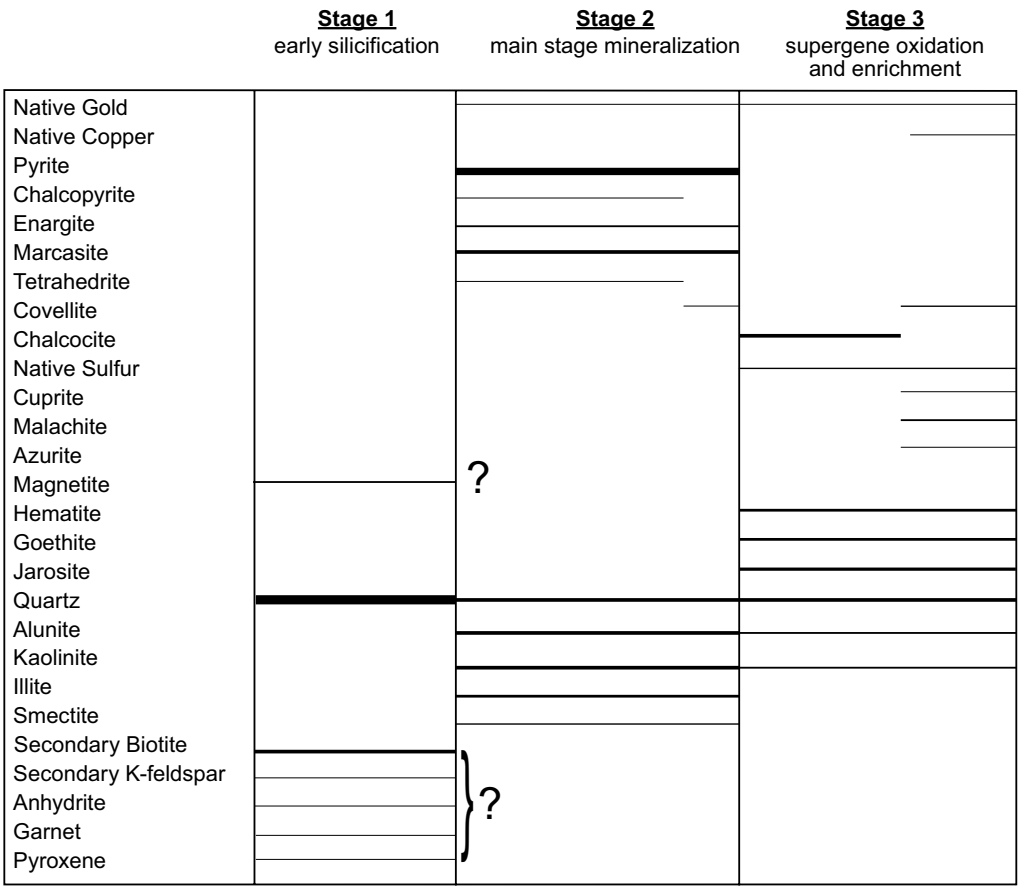

Fig. 7. Paragenetic sequence of the Öksüt Au-Cu deposit.

is also sulfide free, except where it has been partially overprinted by propylitic assemblages containing pyrite (Fig. 8H).

Calc-silicate alteration: Local zones of calc-silicate alteration were observed along the western part of Öksüt within andesitic porphyry and at shallow depths (70–100 m) to the west of Keltepe. Alteration assemblage consists of coarse-grained (up to cm-long), zoned crystals of grossularite alongside diopside and vesuvianite (Fig. 8J-K) developed as infill either along non-planar 1- to 3- cm-thick veinlets or more commonly within open fractures. Retrograde propylitic assemblages including epidote, chlorite, sericite, carbonate, and pyrite generally overprinted this alteration style (Fig. 8K).

Propylitic alteration: Propylitic alteration is not a major constituent of the shallow epithermal system but was ubiquitously developed at deeper levels (> 300 m) marking the peripheries of the magmatic-hydrothermal fluid upflow zones. Abundant epidote and lesser carbonate, pyrite, and chlorite have replaced either the ferromagnesian minerals in precursor pyroxene andesite porphyry or other high-temperature alteration assemblages, including calc-silicate and biotite-magnetite ± K-feldspar±anhdyrite assemblages (Fig. 8H, J, K). Carbonate veinlets with thicknesses of 1 to 2 cm are also commonly present in propylitized andesite porphyry.

Gold-copper mineralization

Öksüt gold-copper mineralization is largely confined to steeply dipping, upward-flaring breccia domains ("ledges") that have been localized along vertical to subvertical faults (Figs. 3A, 5, 6A). Minor gold ± copper mineralization was also identified in the subjacent altered pyroxene andesite porphyry as disseminations. Widths of breccia zones are highly variable, but most have maximum widths of >50 m.

In the Keltepe area, mineralized ledges have been emplaced along a NNW-SSE-trending corridor that is 950 m long and about 500 m wide with a maximum vertical extent of about 400 m. They are either vertical or plunge steeply (50°–75°) to the southeast (Figs. 5, 6). Güneytepe mineralization also follows a similar trend, but its extent is relatively limited; it can be traced over a distance of 350 m along strike, is about 300 m wide, and plunges steeply (~75°) toward the southeast.

The ledges and associated breccias have been oxidized to depths of about 350 m in Keltepe and 110 m in Güneytepe. Consequently, mineralization styles as well as gold-copper grades are strongly zoned (Fig. 5). In the supergene-oxidized zone, fine-grained gold (typically 5–10 μm) occurs within intensely oxidized, silica- or quartz-alunite ± kaolinite-altered, poorly sorted polymict breccias containing abundant goethite and jarosite in the matrix (Fig. 9A-B). The ubiquitous presence of these minerals indicates the former presence of abundant Fe sulfides prior to supergene weathering and that gold was likely liberated after decomposition of pyrite during oxidation. The silicified cores of the breccia feeders return highest average gold grades of >2.5 g/t (up to 30 g/t

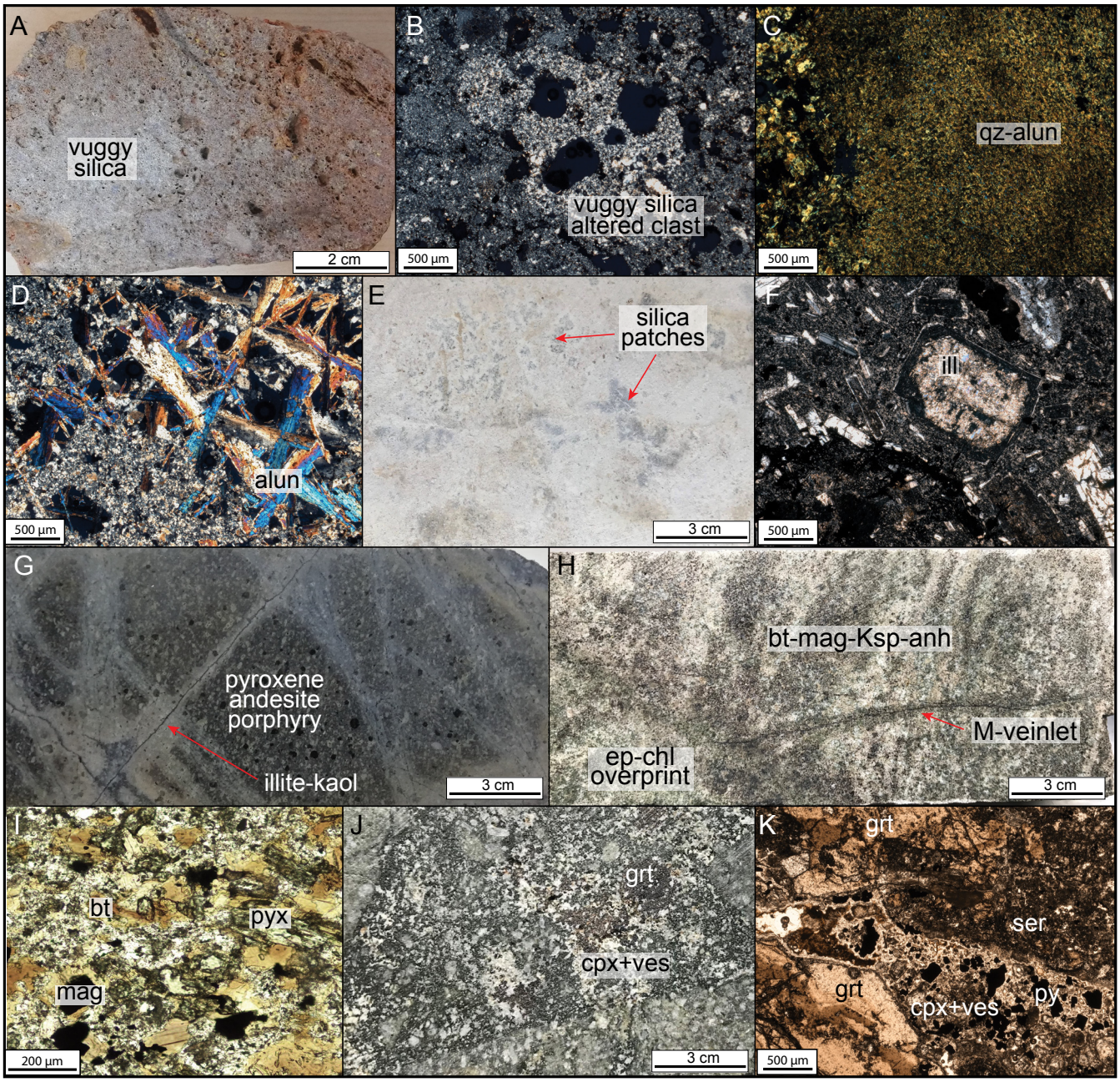

Fig. 8. Various alteration styles in Öksüt. A. Breccia with vuggy residual quartz alteration (ODD-316, 169.00–169.10 m). B. Breccia containing fine-grained vuggy quartz in clasts and matrix (under transmitted light; ODD-316, 116.40–116.50 m). This meter-length interval has an average grade of 2.2 g/t Au. C. Complete replacement of breccia clast by fine-grained quartz-alunite (under transmitted light; ODD-210, 174.10–174.25 m). D. Coarse, prismatic alunite as vug infill (under transmitted light; ODD0210, 182.00–182.10 m). E. Drill core sample showing quartz-alunite alteration with irregular zones of fine-grained patchy silica (ODD-315, 171.50–171.60 m). F. Illite replacement in plagioclase phenocrysts surrounded by a groundmass of quartz-illite-kaolinite-pyrite (under transmitted light; ODD-315, 106.50–106.60 m). G. Pyroxene andesite porphyry crosscut by stockwork veinlets of quartz-pyrite with illite-kaolinite haloes (ODD-315, 220.00–220.10 m). H. Biotite-magnetite-K-feldspar altered pyroxene andesite porphyry crosscut by hairline magnetite (M-type) veinlet, and later overprinted by propylitic (epidote-chlorite) alteration (ODD-337, 706.00–706.30 m). I. Photomicrograph showing intense biotite-magnetite alteration in pyroxene andesite porphyry (under transmitted light; ODD0337, 706.00–706.30 m). J. Fracture filling calc-silicate (grossularite-diopside-vesuvianite) alteration in pyroxene andesite porphyry (ODD-337, 77.30–77.60 m). K. Garnet-diopside-vesuvianite veinlet in pyroxene andesite porphyry. Sericite and pyrite replacement occurred due to retrograde overprint (ODD-337, 71.40–71.80 m). Abbreviations: alun = alunite, anh = anhydrite, bt = biotite, chl = chlorite, ep = epidote, grt = garnet, ill = illite, kaol = kaolinite, Ksp = K-feldspar, mag = magnetite, py = pyrite, pyx = pyroxene, qz = quartz, ser = sericite, ves = vesuvianite.

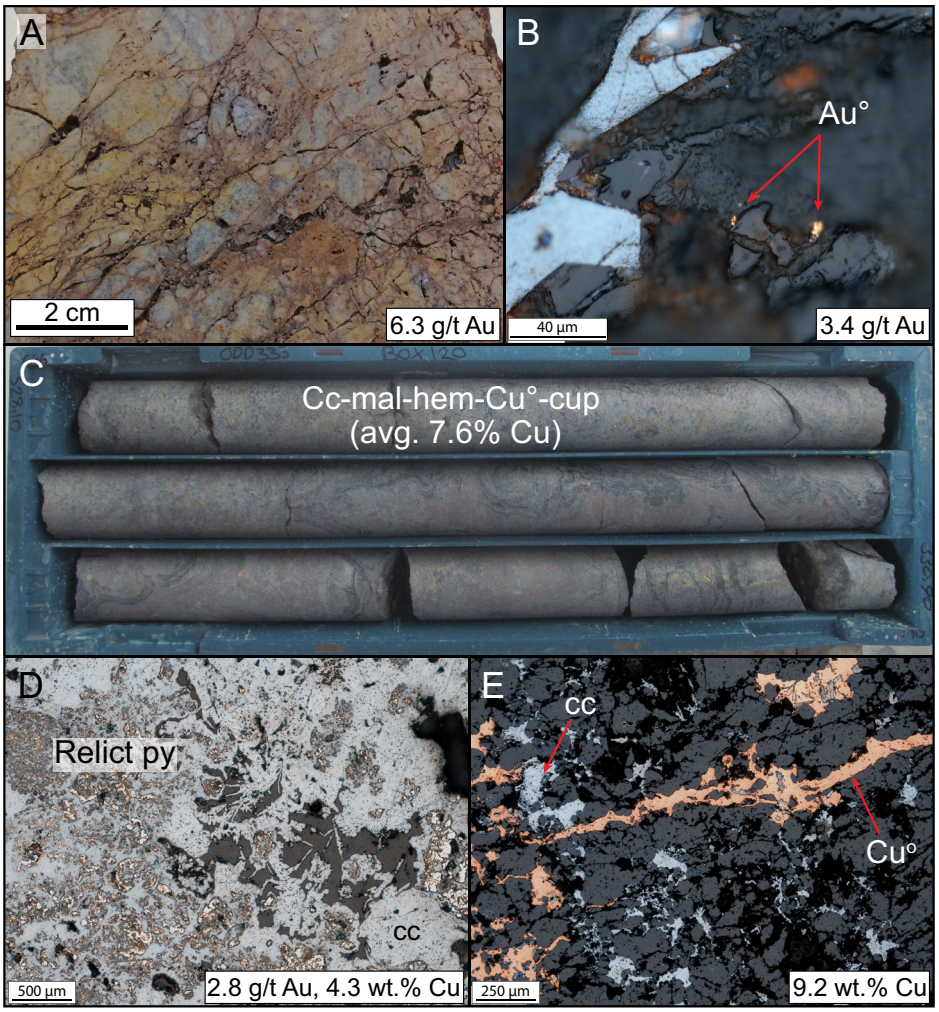

Fig. 9. Representative drill core and photomicrographs of the supergene oxide and enriched sulfide mineralization zones in Öksüt. A. Gold-mineralized silicified breccia with supergene Fe-(hydr)oxides as fracture fill (ODD-316, 104.80–104.90 m). B. Native gold in silicified breccia (ODD-012, 53.20–53.30 m). C. Semimassive chalcocite-rich zone with secondary Cu oxides, Cu hydroxy-carbonates and native copper in alunite-matrix breccia from Keltepe (ODD-333, 328.10–330.90 m). D. Intense chalcocite replacement and relict pyrite (ODD-313, 235.00–235.10 m). E. Chalcocite and fracture filling native copper (ODD0033, 329.75–329.90 m). Abbreviations: cc = chalcocite, cup = cuprite, hem = hematite, mal = malachite, py = pyrite.

Au), whereas quartz-alunite ± kaolinite-altered breccias in the oxidized zone have average gold grades of 1.2 g/t. Copper, however, has been completely leached and redeposited in the quartz-alunite ± kaolinite-altered breccias at the base of the oxidation zone (Figs. 5, 6).

Supergene oxidized portions of the breccia feeders are underlain by an enrichment zone that hosts intervals of significant copper mineralization mainly in quartz-alunite ± kaolinite-altered breccias (Fig. 5A). These comprise predominant chalcocite with subordinate malachite-covellite and sparse azurite, native copper, and cuprite (Fig. 9C-E). Pyrite-marcasite and sparse enargite were also identified as relict hypogene sulfide phases. Presence of relict enargite in the samples suggests that it was the main copper mineral prior to oxidation. Chalcocite occurs as infill to irregular, hairline fractures, as matrix infill in breccia bodies (Fig. 9C), and locally as massive accumulations with pyrite (Fig. 9D). It has been locally replaced by covellite and cuprite along narrow fractures. In the enriched zones, gold grades average around 0.5 g/t.

Enriched horizons are horizontal to subhorizontal (Fig. 5A) and developed irregularly throughout the district. Their thicknesses vary considerably, from 25 to 50 m in the root zones of breccia feeders to <5 m laterally away from the ledges. The chalcocite-pyrite contents may locally range up to over 40 vol %, forming zones of semimassive to massive sulfides (Fig. 9D). The most significant copper enrichment was encountered in drill hole ODD-333 (Fig. 9C), where a ~50-m-thick interval of massive chalcocite-pyrite returned an average grade of 2.3% Cu.

Hypogene mineralization appears at depths >400 m within the ledges (Fig. 5) but is present at much shallower depths (~30 m) outside the breccia zones. It is generally associated with quartz-alunite ± kaolinite alteration (Fig. 10A) and is less commonly present in zones of silicic alteration. In unoxidized breccias, hypogene sulfides including pyrite, marcasite, and enargite primarily occur in the matrices (Fig. 10B-C), less commonly in clasts, and locally as vug fill (Fig. 10D). Outside the ledges, the same mineral assemblage as well as relatively

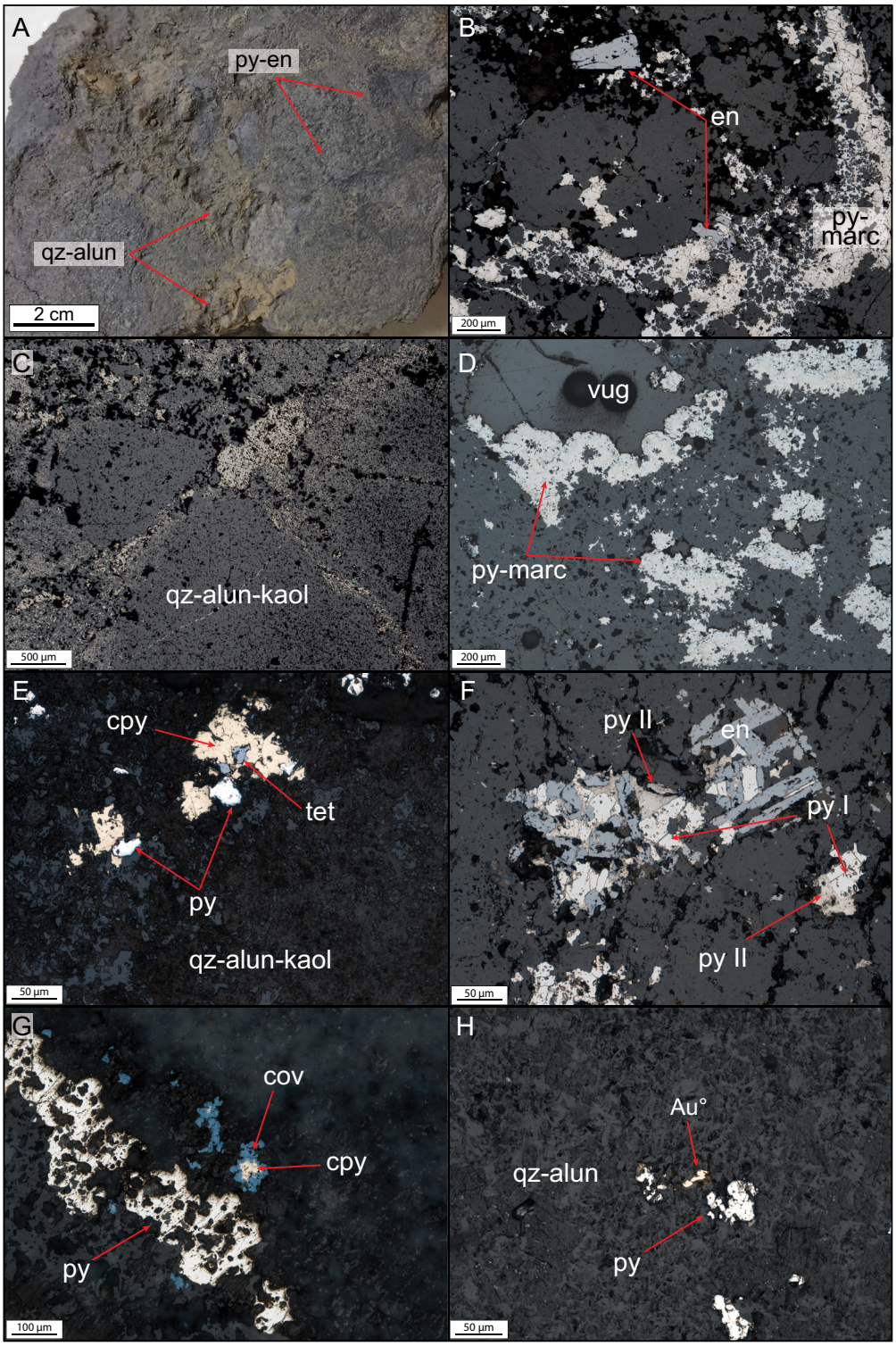

Fig. 10. Representative drill core and photomicrographs of hypogene gold-copper mineralization. A. Quartz-alunite-altered breccia with disseminated pyrite and enargite (ODD-316, 255.30–255.40 m). B. Intergrown pyrite-marcasite-enargite in breccia matrix (ODD-319, 138.40–138.60 m). C. Fine-grained pyrite rimming quartz-alunite-kaolinite-altered breccia clasts. D. Disseminated and vug filling pyrite and colloform marcasite in silica-matrix breccia (ODD-319, 135.50–135.60 m). E. Disseminated pyrite-chalcopyrite-tetrahedrite in quartz-alunite-kaolinite-altered pyroxene andesite porphyry (ODD-033, 131.70–131.80 m). F. Intergrowth of skeletal enargite and pyrite (py I) surrounded and partly replaced by late porous pyrite (py II; ODD-316, 211.60–211.70 m). G. Pyrite ribbon and disseminated chalcopyrite, partially replaced by hypogene covellite. H. Native gold and disseminated pyrite in pyroxene andesite porphyry, showing quartz-alunite alteration (ODD-390, 33.27–33.43 m). Abbreviations: alun = alunite, cc = chalcocite, cov = covellite, cpy = chalcopyrite, en = enargite, kaol = kaolinite, marc = marcasite, py = pyrite, qz = quartz, tet = tetrahedrite.

minor amounts of chalcopyrite, tetrahedrite-tennantite, and sparse hypogene covellite are found as disseminations in pyroxene andesite porphyry (Fig. 10E). Two distinct pyrite varieties were noted in hypogene sulfide zones. Medium-grained, subhedral to anhedral granular pyrite is intergrown with marcasite and tabular prismatic, locally skeletal enargite (Fig. 10F). Early pyrite, marcasite, and enargite have been overgrown by anhedral, often porous looking, sooty pyrite (Fig. 10F). Similar to the enriched levels, gold in hypogene sulfide zones is mostly refractory and occurs as submicron inclusions in pyrite and enargite, and also in pyrite lattice. Native gold is sparse and is generally fine grained (<15 μm; largest observed ~30 μm; Fig. 10H).

Breccias

Öksüt breccias, the main host of gold-copper mineralization, were subdivided into four distinct categories based on detailed core logging and petrography. Within the mineralized zones, a large part of these breccias has undergone intense supergene oxidation, and therefore it is difficult to ascribe a genetic origin for these. Still, a broad distinction was made between early breccia facies (silica-, alunite-, and kaolinite-matrix breccias; Fig. 11A-D) that display phreatomagmatic character and late breccia facies with sulfide-rich matrices (Fig. 11E, F) that rather have mixed hydrothermal-tectonic character. The former group has been observed in both Keltepe and

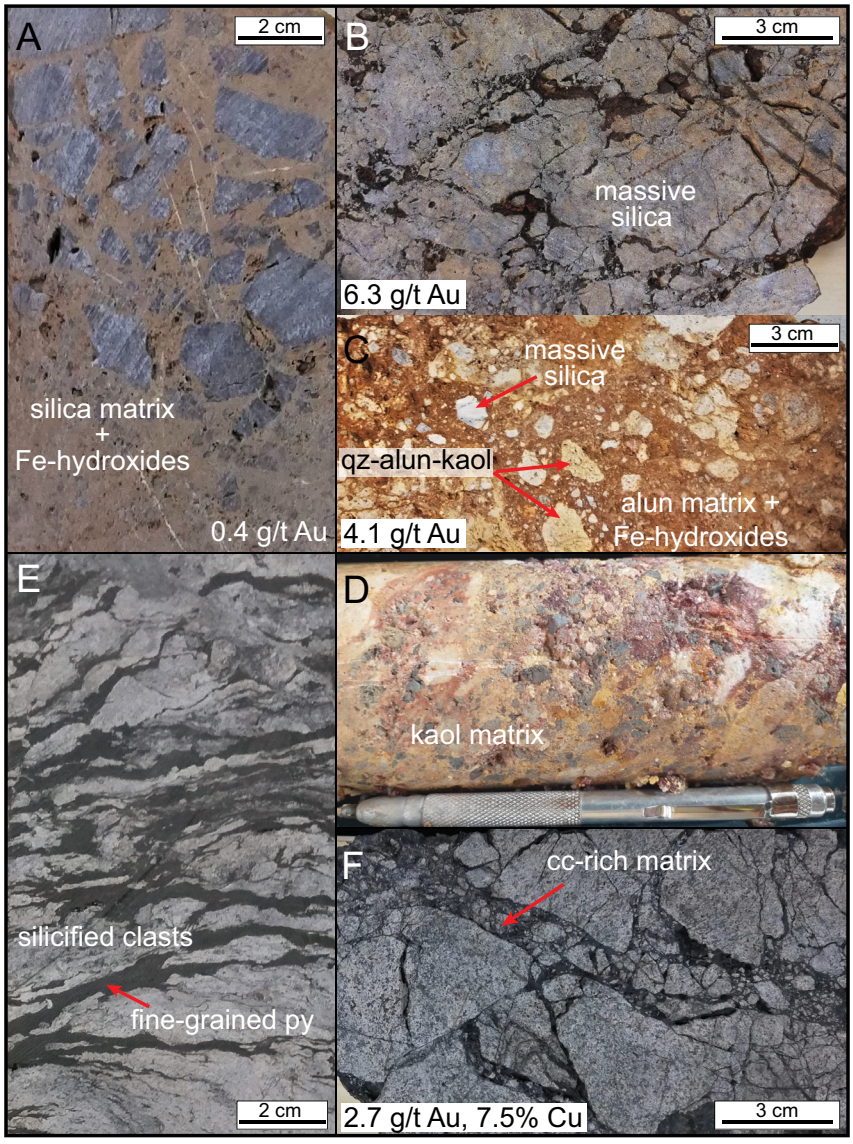

Fig. 11. Breccia types observed in Öksüt. A. Silica-matrix breccia containing clasts showing silicic alteration. Beige color of matrix is due to abundant Fe hydroxides (ODD-012, 33.65–33.80 m). B. Clast-supported massive silica breccia with fracture filling Fe hydroxides (ODD-316, 104.80–104.90 m). C. Matrix-supported alunite-matrix breccia containing fragments of massive silica and quartz-alunite-kaolinite-altered andesite porphyry (ODD-316, 142.00–142.10 m). D. Kaolinite-matrix breccia with rounded to subrounded, silicified fragments (ODD-382, 269.00–269.20 m). E. Sulfide-matrix breccia containing crudely laminated tabular clasts of silicified rock surrounded by fine-grained pyrite (ODD-316, 328.40–328.60 m). F. Jigsaw fit breccia with angular clasts, showing quartz-alunite alteration surrounded by chalcocite-rich matrix (ODD-316, 211.60–211.70 m). Abbreviations: alun = alunite, cc = chalcocite, kaol = kaolinite, qz = quartz.

Güneytepe. These, in places, contain large (several centimeters across) angular fragments within rock-flour matrix, suggesting a diatreme origin (Yıldız et al., 2017).

Silica-matrix breccia: This breccia type is distinguished by abundant silica both in clasts and matrix with or without alunite (Fig. 11A, B). Silica-matrix breccias are matrix- to clast-supported and have angular to subangular, medium- to coarse-grained clasts. They are polymictic in character and contain fragments of massive and vuggy silica as well as of quartz-alunite-altered rocks, where the former clast types dominate (>80% of clasts) over quartz-alunite.

Common hematite/goethite-filled fractures are present in the supergene oxide zone, imparting a typical yellow to reddish brown color to the breccias (Fig. 11B). Such zones return gold grades of up to 4 g/t. On the other hand, at deeper levels massive silica-silica matrix breccias appear in darker colors due to the presence of secondary copper sulfides, such as chalcocite and covellite together with fine-grained pyrite. Consequently, these are associated with significant gold (up to 2.7 g/t Au) and copper (up to 7% Cu) grades.

Alunite-matrix breccia: These are also polymictic, matrix- to clast-supported breccias comprising pervasively quartz-alunite-altered matrices (Fig. 11C). Poorly sorted clasts are fine- to coarse-grained, angular to subangular and include massive to vuggy silica- and quartz-alunite-altered fragments (Fig. 11C), with >60% of these showing quartz-alunite alteration. Altered juvenile fragments of andesite porphyry are also visible, and in places these have cuspate margins (Yıldız et al., 2017). Similar to silica-matrix breccias, alunite-matrix breccias are commonly cut by irregular fractures containing hematite, goethite, and limonite infill at shallow levels in the supergene oxide zone. Overall gold grades are lower than those observed in silica-matrix breccias, and grades of ~2 g/t Au and <0.2% Cu are generally associated with increased secondary iron oxide and hydroxide mineral abundance.

Kaolinite-matrix breccia: These are rare breccias that generally lack gold-copper mineralization. Both clasts and matrix contain abundant clay, dominated by kaolinite (Fig. 11D). Kaolinite-matrix breccias are polymict, matrix to clast supported, and composed of subangular to subrounded clasts. Altered juvenile andesite porphyry fragments have been mainly replaced by quartz-kaolinite, as well as minor amounts of quartz-alunite- and silica-altered fragments.

Sulfide-matrix breccia: Sulfide-matrix breccias were mainly observed in and to the west of Keltepe. They are monomict, clast- to matrix-supported, with clasts predominantly composed of quartz-kaolinite ± alunite-altered andesite porphyry, and sometimes containing quartz-sulfide veinlets. Matrix, on the other hand, is characteristically made up of fine-grained sulfides, either dominated by pyrite or chalcocite (Fig. 11E, F). Where pyrite dominates the matrix, they locally display crude layering with tabular-shaped fragments (Fig. 11E). These are not always associated with significant gold and/or copper, but in places, grades as high as ~0.5 g/t Au and ~0.5% Cu were encountered. Chalcocite-rich sulfide-matrix breccias are usually jig-saw fit, clast-supported breccias (Fig. 11F), and as such, they are associated with elevated copper grades (several percent Cu).

$^{40}Ar/^{39}Ar$ Dating

Two hypogene alunite, one illite, and one hydrothermal biotite separates, all obtained from drill core samples, were dated through $^{40}Ar/^{39}Ar$ step-heating method at the Nevada Isotope Geology Lab of the University of Nevada at Las Vegas, United States. Age uncertainties are reported at 2σ level. Detailed analytical procedures are given in Appendix 1, summary data is provided in Table 1, and age spectra are provided in Figure 11. Full geochronological data are also given in Appendix 2. All samples yielded disturbed and saddle-shaped spectra (Fig. 12A-D).

Sample OD79802 was collected from drill hole ODD-210 from quartz-alunite-kaolinite alteration in Güneytepe and contains coarse (2.5 mm diam), prismatic crystals of hypogene alunite together with quartz, kaolinite, pyrite, and chalcocite. This sample yielded a total gas age of 5.62 ± 0.06 Ma. A second alunite sample (OD79801) collected from an identical drill core interval in Güneytepe returned a total gas age of 7.59 ± 0.09 Ma. The saddle-shaped age spectrum (Fig. 12B) with older early steps suggests the presence of excess argon. Although this sample did not yield a valid plateau age, ~77% of the ^{39}Ar was released in two contiguous steps that have younger apparent ages (Fig. 12B). The lowest step in the saddle with an age of 5.65 ± 0.14 Ma is interpreted to be a maximum age estimate for this sample. This date, which also correlates well with alunite sample OD79802, was taken as the preferred age of this sample.

Drill core sample OD78852 from the argillic zone to the northwest of Keltepe contains a mineral assemblage of illite, quartz, smectite, and pyrite. Illite from this sample returned a total gas age of 5.50 ± 0.34 Ma, correlating with the alunite ages. Steps 5 through 12 contained 69% of the ^{39}Ar released, returning a weighted mean age of 5.26 ± 0.33 Ma (Fig. 12C). The hydrothermal biotite sample (OD78863) from deep biotite-magnetite ± K-feldspar ± anhydrite alteration zone immediately below the argillic alteration from northwest of Keltepe returned a total gas age of 7.41 ± 0.08 Ma, which

Table 1. Summary of $^{40}Ar/^{39}Ar$ Geochronological Data from Hydrothermal Alteration Minerals

Sample no.	Location; drill hole information	Mineral	Occurrence	Total gas age (Ma, 2σ)	Preferred age (Ma, 2σ)
OD78863	Keltepe West; ODD-337; 706.3–706.6 m	Biotite	Biotite-magnetite–K-feldspar-altered pyroxene andesite porphyry	7.41 ± 0.08	-
OD79801	Güneytepe; ODD-210; 179.5–179.6 m	Alunite	Quartz-alunite-kaolinite-altered pyroxene? andesite porphyry	7.59 ± 0.18	5.65 ± 0.14
OD79802	Güneytepe; ODD-210; 182.0–182.1 m	Alunite	Quartz-alunite-kaolinite-altered pyroxene? andesite	5.62 ± 0.06	5.62 ± 0.06
OD78852	Keltepe West; ODD-315; 493.4–493.8 m	Illite	Quartz-illite-smectite-kaolinite	5.50 ± 0.34	5.50 ± 0.34

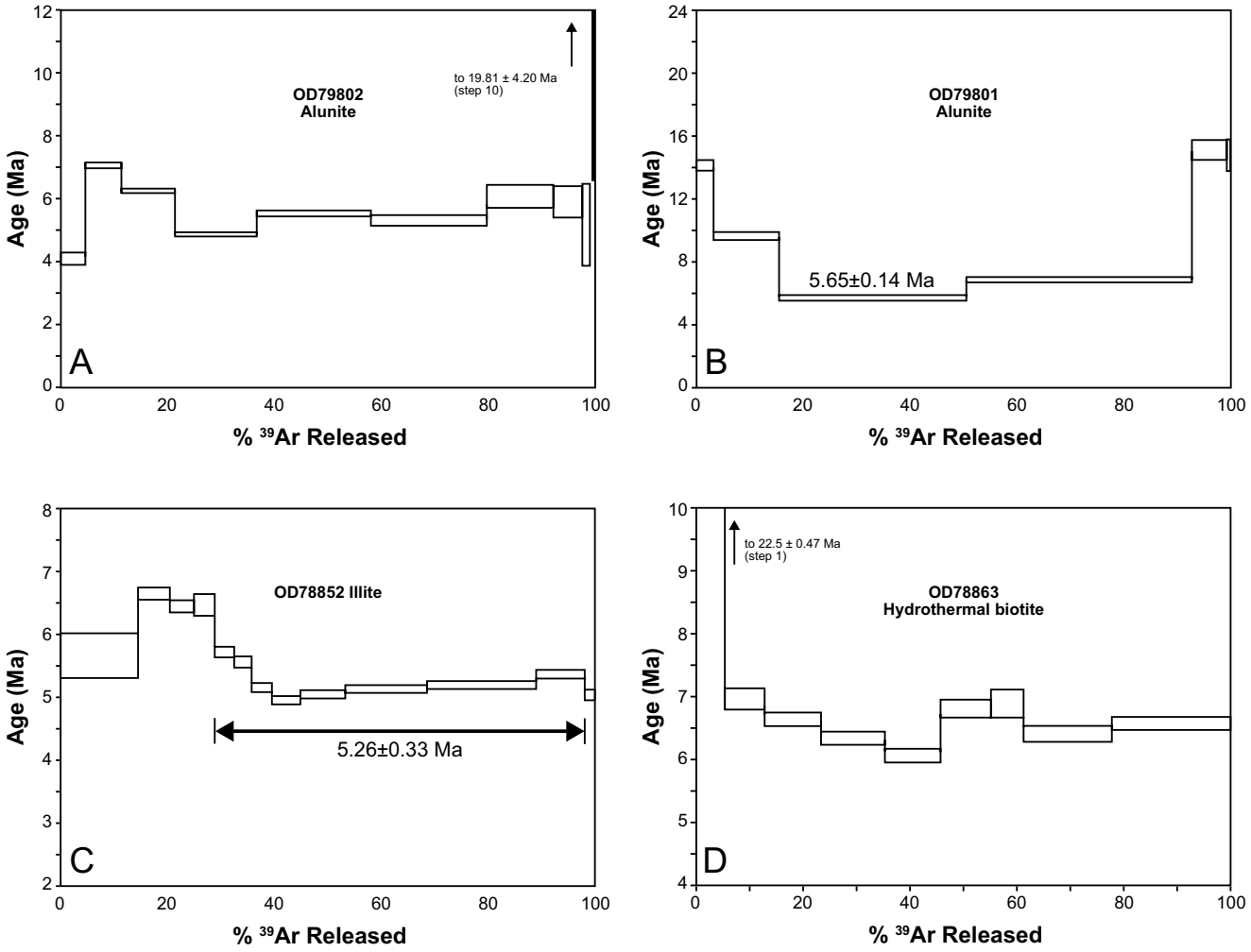

Fig. 12. $^{40}Ar/^{39}Ar$ spectra of alunite, illite, and secondary biotite samples from Öksüt.

is significantly older than the reported ages of least altered andesite porphyry and alteration minerals. This sample also did not produce a plateau. Saddle-shaped age spectra with a hump at moderate temperature steps (Fig. 12) suggests the presence of excess argon. The lowest step with an age of 6.06 ± 0.05 Ma may hint at the maximum age of this sample, which seems reasonable when compared to other samples.

Although no plateau ages could be calculated for the samples, interpreted ages of the three samples obtained from shallow epithermal alteration agree within error (Table 1), and these ages (between 5.7 and 5.5 Ma) approximate the age of alteration associated with gold-copper mineralization. The 5.7 to 5.5 Ma timing also correlates well with the published U-Pb zircon ages of the host pyroxene andesite porphyry (5.7–5.4 Ma; Rabayrol et al., 2019; Aluç et al., 2020).

Discussion

Constraints on formation of hypogene gold-copper mineralization

Öksüt is a typical, breccia-hosted epithermal gold-copper deposit emplaced along a dome-diatreme complex within the Develidağ Volcanic Complex (Yıldız et al., 2017). The host pyroxene andesite porphyry has been partly replaced by zoned alteration sequences characteristic of high-sulfidation epithermal systems. Within this environment, gold-copper mineralization most likely developed through exsolution, channeling and rapid escape of buoyant magmatic vapors along steep structures, some of which are associated with subvertical breccia bodies. As this magmatic vapor phase ascended to the volcanic levels, it evolved into low pH fluids due to condensation into a lower temperature meteoric aquifer (Heinrich, 2005; Hedenquist and Taran, 2013). Further acidification of magmatic vapors is promoted by condensation into local meteoric waters leading to pervasive zoned alteration (Hedenquist et al., 1998; Hedenquist and Taran, 2013). Oxygen and hydrogen isotope compositions of alunite and quartz as well as calculated fluid isotope compositions from Öksüt are consistent with such a mixed magmatic-meteoric, but predominantly magmatic, origin of the fluids (Aluç et al., 2020).

At this stage, the original andesitic wall rock had been completely replaced by massive and residual silica due to decreasing temperature and the low fluid pH, respectively. The outward zonation from central silica alteration through quartz-alunite ± kaolinite to illite-smectite ± chlorite assemblages reflect a decrease in fluid acidity and temperature

(e.g., Stoffregen, 1987; Hedenquist et al., 1994; Hedenquist and Taran, 2013). The upward-flared form of the breccias is attributed to a progressive approach to the paleosurface (Steven and Ratté, 1960; Hedenquist et al., 1994). Gold-copper mineralization was largely introduced subsequently into the same steep structures, with pyrite-enargite-gold overprinting the early residual vuggy and massive silica during the episodic phreatomagmatic brecciation.

The true nature of pyrite-enargite-gold mineralization (primary mineralogy, distribution, and mineral zonation) could not be well-constrained due to the widespread and intense supergene overprinting. Gold-copper mineralization is present in both Keltepe and Güneytepe, where steeply dipping breccias largely confine mineralization. Because highly permeable lithologies such as lacustrine sediments or volcaniclastic units are generally absent in the altered and mineralized stratigraphy, lateral migration of gold-copper mineralization from breccia feeders into enveloping pyroxene andesite porphyry was probably very limited. Thus, epithermal-style hydrothermal alteration and associated mineralization wane typically within just a few tens of meters of these conduits. At the base of the ledges, hypogene mineralization terminates in a zone of illite-smectite-kaolinite alteration and weakly to moderately developed quartz-pyrite-marcasite stockwork veinlets with argillic halos. This alteration assemblage is in turn transitional to a well-developed, albeit barren, potassic (biotite-magnetite ± K-feldspar ± anhydrite) alteration zone at depths greater than 400 m. Altered rocks at these levels contain abundant hydrothermal magnetite, both as disseminations and as M-type veinlets (Fig. 8H, I), a common feature of gold-rich porphyry systems (Sillitoe, 2000; Ulrich and Heinrich, 2002; Perelló et al., 2003). On the other hand, neither sulfide mineralization nor quartz veining, characteristic of porphyry deposits (Sillitoe, 2010), were identified in this zone, and associated gold and copper assays are identical to background values of the least altered rocks.

Geodynamic setting of the Öksüt Au-Cu deposit

In Anatolia, most porphyry and epithermal systems are associated with back-arc, syn- or postcollisional settings (e.g., İmer et al., 2013, 2015; Richards, 2015; Kuşcu et al., 2019; Rabayrol et al., 2019). Our new $^{40}Ar/^{39}Ar$ alunite and illite ages (Table 1, Fig. 12) from Keltepe and Güneytepe, combined with previously reported zircon U-Pb ages of Rabayrol et al. (2019) and Aluç et al. (2020) from the host pyroxene andesite porphyry, confirm the ~5.7 to 5.5 Ma age for formation of high-sulfidation epithermal mineralization at Öksüt. The timing of magmatism and epithermal-style alteration at Öksüt postdates the early to middle Miocene closure of the southern Neotethys Basin (Okay et al., 2010), which serves as unequivocal evidence for formation in a postsubduction setting. According to Aluç et al. (2020), epithermal-style mineralization at Öksüt is mainly hosted in the hornblende-phyric dacite porphyry, and that the duration of mineralization was short-lived (<80 kyr) as constrained by the mean U-Pb zircon age of this unit (5.73 ± 0.06 Ma) and the youngest U-Pb zircon age (5.67 ± 0.07 Ma) of the overlying pyroxene andesite porphyry. However, our field, drill core, and petrographic observations, as well as interpreted $^{40}Ar/^{39}Ar$ ages, indicate that mineralization was rather coeval with the emplacement of pyroxene andesite porphyry and its timing likely extended at least to 5.5 Ma.

Epithermal-style alteration and gold-copper mineralization developed coevally with andesitic volcanism at the Develidağ Volcanic Complex during regional-scale extension along the Ecemiş corridor (Fig. 2; Koçyiğit and Erol, 2001; Jaffey et al., 2004). The ~5.7 to 5.5 Ma formation age also makes Öksüt the youngest major gold deposit in Anatolia, and possibly in the entire western Tethyan metallogenic belt. The older hydrothermal biotite total gas age of ~7.4 Ma (Table 1) from biotite-magnetite-K-feldspar-altered pyroxene andesite porphyry west of Keltepe does not agree with the U-Pb zircon age of the same unit (Rabayrol et al., 2019; Aluç et al., 2020), and is therefore considered unreliable. Another, but less likely explanation is that biotite-magnetite ± K-feldspar ± anhydrite alteration is associated with an earlier phase of magmatism, previously not recognized in the Develidağ Volcanic Complex. A pyroxene andesite porphyry unit with a slightly older U-Pb zircon age of 7.9 ± 0.14 Ma was reported from the Tekkedağ volcanic suite (Rabayrol et al., 2019), situated approximately 45 km to the northwest (Fig. 2). Still, due to the absence of porphyry-altered/mineralized clasts in phreatomagmatic breccias or evidence for late overprinting of biotite-magnetite ± K-feldspar±anhydrite alteration by epithermal assemblages, we tentatively infer that both epithermal and porphyry alteration styles at Öksüt developed contemporaneously as part of the same magmatic-hydrothermal event.

The late Miocene-early Pliocene magmatism at the Develidağ Volcanic Complex and throughout south-central Anatolia was a result of either postcollisional rollback of the Cyprian slab or delamination beneath central Anatolia (Rabayrol et al., 2019). Both scenarios involve remelting of previously modified subarc lithosphere to form calc-alkaline magmas that compositionally mimic those observed in continental arcs. Consequently, Richards (2009, 2011) suggested that such magmas may generate postsubduction Au-rich porphyry and epithermal systems through remobilization of sulfide phases normally retained in deep root sections of arcs.

Formation of porphyry deposits depends on a number of successive processes, from melt generation at depth through magma emplacement in mid- to upper-crustal levels, to ultimate ore deposition around shallowly emplaced intrusions. Unless these processes operate optimally, the chances of forming an economic porphyry system are likely to be low (e.g., Richards, 2003; Sillitoe, 2010). Source magmas of the late Miocene volcanic centers in south-central Anatolia are hydrous and oxidized and are therefore deemed to be potentially fertile for porphyry-style mineralization (Kuşcu et al., 2019; Rabayrol et al., 2019). In the presence of favorable magma compositions, evolution of upper-crustal magma chambers and style of magmatism play a vital role in later stages of fluid exsolution and sulfide precipitation. Transpressional or transtensional strain across arc segments or collisional to postcollisional settings are regarded as prerequisites for porphyry development (Tosdal and Richards, 2001), since such conditions promote efficient convective crystallization of magmas leading to volatile saturation and magmatic fluid exsolution (e.g., Shinohara and Hedenquist, 1997; Richards, 2003; Wilkinson, 2013). Notable exceptions to this are synextensional porphyry districts formed after crustal overthickening, as observed along the Miocene

Gangdese belt in Tibet (Hou et al., 2009), the Cretaceous Zijinshan district in southeast China (Piquer et al., 2017), the Eocene Biga Peninsula in northwest Anatolia (Sánchez et al., 2016), and probably also in the Kışladağ porphyry Au deposit in western Anatolia (Baker et al., 2016). Nevertheless, no major period of crustal thickening was recorded around the Ecemiş sector of the central Anatolian fault zone prior to the late Miocene, and thus, the prevalent extensional stress regime and explosive nature of Develidağ Volcanic Complex magmatism during Öksüt mineralization is hereby considered to be unfavorable for porphyry-style mineralization. This would explain the overall lack of quartz veining and sulfide precipitation in the biotite-magnetite ± K-feldspar ± anhydrite alteration zone, as well as the absence of phyllic alteration beneath both Keltepe and Güneytepe.

Regional significance and relation to Late Cenozoic central Anatolian tectonism

Late Cenozoic postsubduction magmatism along south-central and adjacent western Anatolian areas is considered to be highly productive in terms of gold mineralization. The latter region features some important gold ± copper deposits (e.g., Kışladağ; Figs. 1, 13, Table 2) and its mineralization potential has been outlined through detailed exploration. In contrast, the extent of gold mineralization along the late Miocene-Pliocene volcanic belt in south-central Anatolia has not been constrained in detail, not least because this belt received little exploration until the work by Stratex during the last decade (Yıldız et al., 2017). Large areas of hydrothermally altered rock are present but apart from Öksüt, the only economically important systems recognized to date are the İnlice high-sulfidation (proven and probable reserves: 0.25 Moz) and Himmetdede low-sulfidation (proven and probable reserves plus inferred resource: 0.95 Moz) epithermal gold mineralizations.

Himmetdede, situated ~80 km to the northwest (Fig. 1), is a metamorphic rock-hosted low-sulfidation Au deposit of unknown but probable late Cenozoic age (Table 2). Hypogene gold mineralization at Himmetdede is mainly contained in quartz-dominant, sulfide-poor, pyritic breccias, and was likely sourced from a deep-seated intrusion laterally offset from the deposit. In these aspects, it differs significantly from the rest of the gold mineralized systems of the south-central Anatolian volcanic belt, and rather bears similarities to the low-temperature, breccia- and vein-hosted Sb-Hg-Ag deposits of the Niğde metamorphic massif (Fig. 1), also associated with distal Miocene granitoids (Akçay, 1995).

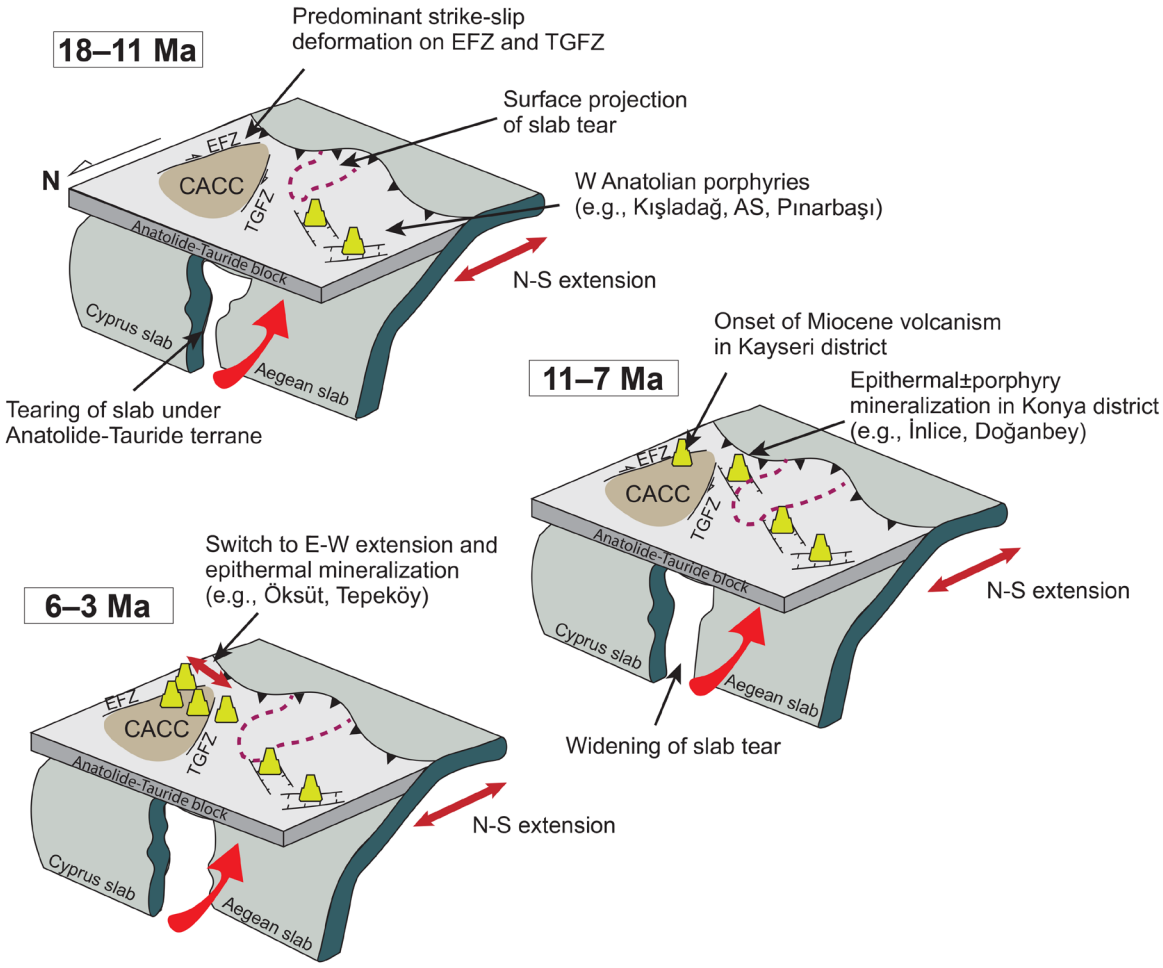

Fig. 13. Cartoon illustrating the temporal evolution of late Cenozoic (middle to late Miocene-early Pliocene) gold-copper mineral districts in south central and western Anatolia in relationship to regional tectonics. Abbreviations: CACC = Central Anatolian Crystalline Complex, EFZ = Ecemiş fault zone, TGFZ = Tuz Golu fault zone.

Table 2. Summary Characteristics of Late Cenozoic Gold Systems in South Central and Western Anatolia

	Kayseri district		Konya district		Afyon-Uşak district	
	Öksüt	Himmetdede	Doğanbey	İnlice	AS	Kışladağ
Geologic setting	Remnant caldera	Concealed subvolcanic intrusion (dome?)	Volcanic dome	Volcanic dome	Intrusive stock	Stratovolcano
Basement	Tauride carbonate	Kırşehir massif	Tauride carbonate	Tauride carbonate	Menderes massif	Menderes massif
Formation	Develidağ VC	Bozçaldağ formation	Erenlerdağ VC	Erenlerdağ VC	Afyon volcanics	Beydağı stratovolcano
Host rock	Andesite porphyry, diatreme	Gneiss, schist, marble	Trachyte, tuff, ignimbrite (3)	Rhyolite, trachyte-latite porphyry	Monzonite, syenite	Monzonite, trachyte, latite
Stress regime	Extensional	Extensional	Extensional	Extensional	Extensional	Extensional
Regional structure	Ecemiş FZ	None recognized; local-scale normal and thrust faults	Akşehir-Afyon FZ	Akşehir-Afyon FZ	Sandıklı graben	Uşak-Güre graben
Mineralization style	HS epithermal Au-Cu	LS epitherma Au	Porphyry Cu-Mo-Au	HS epithermal Au	Porphyry Cu-Au	Porphyry Au
Ore minerals	Au, Cu, cpy, py, mar, tet, en, cc, cov, mal, azur, cup, mag	Py, sph, gn, mar	Cpy, py, mol, mag	Au, Cu, cpy, py, en, sph, cc, cov, mal, bn	Py, tet, cpy, bn, moly, cov, mag, mal, azur	Au, py, sph, mar, moly, tet-ten, bnnt, cpy
Ore textures	Vuggy to massive quartz, breccia, disseminations	Breccia	Veinlets	Vuggy quartz, breccias, veins	Breccias, vein(let)s, disseminations	Stockwork veinlets, disseminations, breccias
Main alteration styles	Silicification, advanced argillic, argillic, potassic	Silicification, argillic	Silicification, advanced argillic, argillic	Silicification, advanced argillic, argillic	Potassic, phyllic, advanced argillic, propylitic	Potassic, phyllic, advanced argillic
Alteration age	5.7–5.5 Ma	-	Miocene	Miocene	11.2 Ma	14.5–13.8 Ma
Supergene oxidation	To 400 m depth	Deep (unreported)	-	~40 m	200 m	Shallow
Host rock age	5.7–5.4 Ma (2)	Middle to late Miocene?	Miocene	8.98 Ma	12.5–10.5 Ma	14.8–14.4 Ma
Data sources	1, 2, this study		1, 3, 4	1, 3, 4	1, 3, 5	1, 6

Data sources: 1 = Rabayrol et al. (2019), 2 = Aluç et al. (2020), 3 = Kuşcu et al. (2019), 4 = Hall et al. (2007), 5 = Sönmez and Kuşcu (2020), 6 = Baker et al. (2016)

Abbreviations: azur = azurite, bn = bornite, bnnt = bournonite, cpy = chalcopyrite, cup = cuprite, FZ = fault zone, gn = galena, HS = high-sulfidation, LS = low-sulfidation, mag = magnetite, mal = malachite, mar = marcasite, moly = molybdenite, py = pyrite, sph = sphalerite, ten = tennantite, tet = tetrahedrite, VC = volcanic complex

İnlice is located approximately 300 km to the west of Öksüt and lies within the Konya volcanic district (Fig. 1). It is, in most aspects, analogous to the Öksüt deposit. Mineralization is hosted by older (~9 Ma; Kuşcu et al., 2019; Rabayrol et al., 2019) calc-alkaline andesites and is confined to steeply dipping silica ledges with surrounding advanced argillic alteration (Hall et al., 2007). Supergene oxidation was only shallowly (<40 m) developed at İnlice and the overall system lacks copper mineralization and deeper porphyry-style alteration (Hall et al., 2007). The nearby Doğanbey porphyry Cu-Mo-Au prospect, situated about 16 km northwest of İnlice, is the only known porphyry occurrence throughout the entire extent of the Miocene-Pliocene belt in south-central Anatolia. Porphyry-style mineralization at Doğanbey occurs within potassic-altered pyroxene andesite porphyries (~10 Ma; Kuşcu et al., 2019; Rabayrol et al., 2019) concealed beneath a gold-mineralized lithocap (Hall et al., 2007). Both İnlice and Doğanbey were regionally controlled by the NW-trending Akşehir fault zone (Fig. 1), which according to Koçyiğit et al. (2000) accommodated a period of mild compression during the late Miocene, coincident with mineralization in these localities. This is in contrast to the predominantly extensional stress regime that prevailed during the late Miocene along the Ecemiş corridor. For the reasons explained above, the general tectonic setting of the Konya volcanic district may thus be more conducive for upper-crustal magma chamber development and porphyry-style mineralization.

Volcanism in the Melendiz area (Fig. 1), on the other hand, is younger (5–3 Ma; Rabayrol et al., 2019) than that of Konya, Develidağ Volcanic Complex, and Tekkedağ areas. It contains few high-sulfidation epithermal prospects including Tepeköy, Boztepe, and Altunhisar (Fig. 1). The Tepeköy prospect is hosted within Miocene pyroxene-bearing andesite porphyries exposed in a stratovolcano setting. A K/Ar age of 4.2 ± 0.4 Ma was reported from Tepeköy (Türkecan et al., 2003), but the age of hydrothermal alteration is not known. The emplacement of the volcanic sequence at Tepeköy was controlled by the Tuz Gölü fault zone (Fig. 1), which is conjugate to the Ecemiş fault zone such that it similarly accommodated extension in the late Miocene (Koçyiğit and Beyhan, 1998).

Farther to the west, in western Anatolia, middle Miocene magmatism generated the world-class Kışladağ porphyry Au deposit and few important prospects, such as the AS Cu-Au and Pınarbaşı Cu-Mo porphyry systems (Figs. 1, 13; Table 2). These porphyry systems formed between 18 and 11 Ma (Baker et al., 2016; Delibaş et al., 2017; Kuşcu et al., 2019; Rabayrol et al., 2019; Sönmez and Kuşcu, 2020), in relationship to postsubduction rollback of the Aegean slab and N-S-directed propagation of a slab tear to the west of the Konya volcanic district (Fig. 13). Under such stress conditions, E-W- and NW-SE-trending grabens acted as the major foci of magmatism and porphyry-style mineralization (Fig. 13; Table 2). The nature of Miocene magmatism in western Anatolia was mostly

calc-alkaline, but the AS porphyry prospect is hosted within ~11 Ma alkaline intrusions developed on the western edge of the slab tear (Rabayrol et al., 2019; Sönmez and Kuşcu, 2020). No economic high-sulfidation epithermal system akin to Öksüt or İnlice has been discovered in this part of the belt so far, but this appears to be circumstantial and not directly related to regional tectonics or style of magmatism. Conversely, the south-central Anatolian tectonics during the late Miocene was controlled predominantly by transtensional or transpressional strike-slip fault systems (e.g., Ecemiş, Tuz Gölü, and Akşehir fault zones; Fig. 1) along which intermittent episodes of relaxation and extension led to development of high-sulfidation epithermal Au mineralization (Fig. 13). Therefore, we consider the geodynamic conditions that led to formation of Öksüt to be considerably different in comparison to those responsible for the porphyry-style mineralization in western Anatolia.

Deep oxidation of the epithermal system

At Öksüt, supergene oxidation locally extends to depths of >300 m and it was fundamental to development of economic gold mineralization (Yıldız et al., 2017). Oxidation to similar or greater depths of >300 m has also been observed in some other important epithermal systems, particularly in the central Andes (Sillitoe, 2005). However, similar examples are not known in Turkey. As such, deep supergene oxidation is hereby regarded as a distinctive feature of the Öksüt high-sulfidation epithermal system among its Anatolian counterparts and appears to have resulted from a combination of both district- and regional-scale factors.

Major factors that contributed to deep oxidation of the Öksüt Au-Cu deposit are the subvertical, tabular, and permeable nature of the mineralized breccias, topographically prominent position of the Develidağ Volcanic Complex, and late Miocene to Recent >2-km uplift of the south-central Anatolian margin (Schildgen et al., 2012; Yıldız et al., 2017). The first reason likely enhanced groundwater descent through breccia feeders, whereas the other two resulted in a deep water table, enhancing sulfide enrichment by exposing zones of hypogene sulfides to oxidation. Consequently, refractory gold was liberated from sulfide minerals, making much of the gold-mineralized orebody amenable to cyanide leaching. In addition, copper was significantly redistributed and enriched into locally up to 50-m-thick but discontinuous chalcocitic zones, while arsenic was removed from the pyrite-enargite-gold ores.

Conclusions

The Öksüt gold-copper deposit formed at ~5.7 to 5.5 Ma during the emplacement of the Develidağ Volcanic Complex in south-central Anatolia. The close agreement between the ages of alteration minerals and that of the host andesite porphyry indicates contemporaneous development of late Miocene postsubduction volcanism and high-sulfidation epithermal Au-Cu mineralization. Öksüt formation was also coincident with the onset of E-W-directed extension along the Ecemiş corridor, and that mineralization is closely associated with the vertical to subvertical faults developed in response to this extensional regime. Our reported ages confirm this largest known gold system in central Anatolia as the youngest epithermal deposit in the western Tethyan metallogenic belt.

Gold-copper mineralization is primarily hosted by structurally controlled breccia domains. These breccias are concentrated within the Keltepe and Güneytepe orebodies and show zoned alteration from a central silica through quartz-alunite-kaolinite to kaolinite-illite/smectite alteration at the peripheries. Gold is hosted in both of silica and quartz-alunite-kaolinite, where it is associated with a predominantly hypogene assemblage of pyrite, enargite, and marcasite. Deeper kaolinite-illite/smectite and locally developed biotite-magnetite ± K-feldspar ± anhydrite alteration zones, on the other hand, are devoid of any mineralization.

The gold potential at Öksüt is a result of the deeply oxidized nature of the hydrothermal system. This was interpreted to be a consequence of several factors, including significant surface uplift (>2 km) since the late Miocene, increased permeability of breccia zones for descending groundwaters, and deeply incised topography exposing parts of the hydrothermal system to weathering. As a consequence, supergene weathering locally extended to depths of >300 m, generating gold-mineralized, silica and iron-hydroxide-rich breccias, and making Öksüt mineralization amenable to standard heap-leach methods. Copper, on the other hand, was largely redistributed in chalcocite zones beneath the oxidized gold ore.

Acknowledgments

This work was undertaken as part of an M.Sc. research project by the first author. We would like to thank Centerra Gold for financial and logistical support. Particular thanks are due to Malcolm Stallman for his overall support, Deniz Can Serçe and Semih Bekarslan for helpful discussions on Öksüt mineralization, Ayşegül Dağgez for TerraSpec readings, and Simge Cavunt for help with GIS data. We also thank Kathleen Zanetti of the Nevada Isotope Geochronology Laboratory (UNLV) for Ar-Ar isotope analyses. Finally, we thank editors Rui Wang for handling of the manuscript and Ali Sholeh for comments and suggestions. Further valuable suggestions and corrections provided by Richard Sillitoe, Bahri Yıldız, and an anonymous reviewer significantly improved the manuscript.

REFERENCES

Akçay, M., 1995, Geological and mineralogical investigation of the Gümüşler (Niğde) Sb ± Hg ± W occurences and implications on their gold potential: Geological Bulletin of Turkey, v. 38, p. 23–34.

Aluç, A., Kuşcu, İ., Peytcheva, I., Cihan, M., von Quadt, A., 2020, The late Miocene Öksüt high sulfidation epithermal Au-Cu deposit, central Anatolia, Turkey: Geology, geochronology, and geochemistry: Ore Geology Reviews, v. 126, 103795.

Arancibia, O., and Clark, A.H., 1996, Early magnetite-amphibole-plagioclase alteration-mineralization in the Island Copper porphyry copper-gold-molybdenum deposit, British Columbia: Economic Geology, v. 91, p. 402–438.

Aydar, E., Schmitt, A.K., Çubukçu, H.E., Akin, L., Ersoy, O., Sen, E., Duncan, R.A., and Atici, G., 2012, Correlation of ignimbrites in the central Anatolian volcanic province using zircon and plagioclase ages and zircon compositions: Journal of Volcanology and Geothermal Research, v. 213, p. 83–97.

Baker, T., Bickford, D., Juras, S., Lewis, P., Oztas, Y., Ross, K., Tukac, A., Rabayrol, F., Miskovic, A., Friedman, R., Creaser, R.A., and Spikings, R., 2016, The geology of the Kisladag porphyry gold deposit: Society of Economic Geology Special Publication 19, p. 57–83.

Bartol, J., and Govers, R., 2014, A single cause for uplift of the central and eastern Anatolian Plateau?: Tectonophysics, v. 637, p. 116–136.

Besang, C., Eckhardt, F.J., Harre, W., Kreuzer, H., and Müller, P., 1977, Radiometrische altersbestimmungen an neogenen eruptivgesteinen der Türkei: Geologisches Jahrbuch B, v. 25, p. 3–36.

Cihan, M., Serçe, D.C., and Bekarslan, S., 2016, Öksüt gold project: From grassroots to reserve and forward to mine development: Society of Economic Geologists 2016 Conference, Tethyan Tectonics and Metallogeny, September 25–28, 2016, Çeşme, Turkey, Proceedings, 1 p.

Cosentino, D., Schildgen, T.F., Cipollari, P., Faranda, C., Gliozzi, E., Hudáčková, N., and Strecker, M.R., 2012, Late Miocene surface uplift of the southern margin of the central Anatolian Plateau, central Taurides, Turkey: Geological Society of America Bulletin, v. 124, p. 133–145.

Delibaş¸, O., Moritz, R., Chiaradia, M., Selby, D., Ulianov, A., and Revan, M.K., 2017, Post-collisional magmatism and ore-forming systems in the Menderes massif: New constraints from the Miocene porphyry Mo-Cu Pınarbaşı system, Gediz-Kütahya, western Turkey: Mineralium Deposita, v. 52, p. 1157–1178.

Delph, J.R., Abgarmi, B., Ward, K.M., Beck, S.L., Ozacar, A.A., Zandt, G., Sandvol, E., Turkelli, N., and Kalafat, D., 2017, The effects of subduction termination on the continental lithosphere: Linking volcanism, deformation, surface uplift, and slab tearing in central Anatolia: Geosphere, v. 13, p. 1–18.

Gençalioğlu-Kuşcu, G., and Geneli, F., 2010, Review of post-collisional volcanism in the central Anatolian Volcanic Province (Turkey), with special reference to the Tepekoy Volcanic Complex: International Journal of Earth Sciences, v. 99, p. 593–621.

Göğüş, O.H., Pysklywec, R.N., Şengör, A.M.C., and Gün, E., 2017, Drip tectonics and the enigmatic uplift of the central Anatolian Plateau: Nature Communications, v. 8, 1538, https:// doi .org /10.1038 /s41467-017-01611-3.

Hall, D.J., Foster, R.P., Yildiz, B., and Redwood, S.D., 2007, The Inlice high-sulphidation epithermal gold discovery: Defining a potential new gold belt in Turkey: Biennial Meeting of the Society for Geology Applied to Mineral Deposits (SGA), 9th, Dublin, Ireland, August 20–23, 2007, Proceedings, p. 113–116.

Hedenquist, J.W., and Taran, Y.A., 2013, Modeling the formation of advanced argillic lithocaps: Volcanic vapor condensation above porphyry intrusions: Economic Geology, v. 108, p. 1523–1540.

Hedenquist, J.W., Matsuhisa, Y., Izawa, E., White, N.C., Giggenbach, W.F., and Aoki, M., 1994, Geology and geochemistry of high-sulfidation Cu-Au mineralization in the Nansatsu district, Japan: Economic Geology, v. 89, p. l–30.

Hedenquist, J.W., Arribas, A., Jr., and Reynolds, T.J., 1998, Evolution of an intrusion-centered hydrothermal system: Far Southeast Lepanto porphyry and epithermal Cu-Au deposits, Philippines: Economic Geology, v. 93, p. 373–404.

Heinrich, C.A., 2005, The physical and chemical evolution of low-salinity magmatic fluid at the porphyry to epithermal transition: A thermodynamic study: Mineralium Deposita, v. 39, p. 864–889.

Hou, Z., Yang, Z., Qu, X., Meng, X., Li, Z., Beaudoin, G., Rui, Z., Gao, Y., and Zaw, K., 2009, The Miocene Gangdese porphyry copper belt generated during post-collisional extension in the Tibetan orogen: Ore Geology Reviews, v. 36, p. 25–51.

Imer, A., Richards, J.P., and Creaser, R.A., 2013, Age and tectonomagmatic setting of the Eocene Çöpler-Kabataş magmatic complex and porphyry-epithermal Au deposit, east-central Anatolia, Turkey: Mineralium Deposita, v. 48, p. 557–583.

Imer, A., Richards, J.P., Creaser, R.A., and Spell, T.L., 2015, The late Oligocene Cevizlidere Cu-Au-Mo deposit, Tunceli Province, eastern Turkey: Mineralium Deposita, v. 50, p. 245–263.

Innocenti, F., Mazzuoli, R., Pasquarè, G., Radicati Di Brozolo, F., and Villari, L., 1975, The Neogene calcalkaline volcanism of central Anatolia: Geochronological data on Kayseri-Nigde area: Geological Magazine, v. 112, p. 349–360.

Jaffey, N., and Robertson, A.H.F., 2001, New sedimentological and structural data from the Ecemis fault zone, southern Turkey: Implications for its timing and offset and the Cenozoic tectonic escape of Anatolia: Journal of the Geological Society, London v. 158, p. 367–378.

Jaffey, N., Robertson, A.H.F., and Pringle, M., 2004, Latest Miocene and Pleistocene ages of faulting, determined by $^{40}Ar/^{39}Ar$ single-crystal dating of airfall tuff and silicic extrusives of the Erciyes Basin, central Turkey: Evidence for intraplate deformation related to the tectonic escape of Anatolia: Terra Nova, v. 16, p. 45–53.

Koçyiğit, A., and Beyhan, A., 1998, A new intracontinental transcurrent structure: the central Anatolian fault zone, Turkey: Tectonophysics, v. 284, p. 317–336.

Koçyiğit, A., and Erol, O., 2001, A tectonic escape structure: Erciyes pull-apart basin, Kayseri, central Anatolia, Turkey: Geodinamica Acta, v.14(1), p. 133–145.

Koçyiğit, A., Ünay, A., and Saraç, G., 2000, Episodic graben formation and extensional neotectonic regime in west central Anatolia and the Isparta Angle: A case study in the Akşehir-Afyon graben, Turkey: Geological Society of London Special Publication 173, p. 405–421.

Kürkcüoglu, B., 2010, Geochemistry and petrogenesis of basaltic rocks from the Develidağ volcanic complex, central Anatolia, Turkey: Journal of Asian Earth Science, v. 37, p. 42–51.

Kuşcu, İ., Tosdal, R., and Gençalioğlu-Kuşcu, G., 2019, Episodic porphyry Cu (-Mo-Au) formation and associated magmatic evolution in Turkish Tethyan collage: Ore Geology Reviews, v. 107, p. 119–154.

MTA, 2002, Geological map of Turkey: Ankara, Turkey, Maden Tetkik ve Arama Genel Müdürlüğü (MTA), scale 1:500,000.

Okay, A.İ., Zattin, M., and Cavazza, W., 2010, Apatite fission-track data for the Miocene Arabia-Eurasia collision: Geology, v. 38, p. 35–38.

Pasquare, G., Poli, S., Vezzoli, L., and Zanchi, A., 1988, Continental arc volcanism and tectonic setting in central Anatolia, Turkey: Tectonophysics, v. 146, p. 217–230.

Perelló, J., Carlotto, V., Zárate, A., Ramos, P., Posso, H., Neyra, C., Caballero, A., Fuster, N., and Muhr, R., 2003, Porphyry-style alteration and mineralization of the middle Eocene to early Oligocene Andahuaylas-Yauri belt, Cuzco region, Peru: Economic Geology, v. 98, p. 1575–1605.

Piquer, J., Cooke, D.R., Chen, J., and Zhang, L., 2017, Synextensional emplacement of porphyry Cu-Mo and epithermal mineralization: the Zijinshan district, southeastern China: Economic Geology, v. 112, p. 1055–1074.

Rabayrol, F., Hart, C., and Creaser, R.A., 2019, Tectonic triggers for post-subduction magmatic-hydrothermal gold metallogeny in the late Cenozoic Anatolian Metallogenic Trend, Turkey: Economic Geology, v. 114, p. 1339–1363.

Reid, M.R., Schleiffarth, W.K., Cosca, M.A., Delph, J.R., Blichert-Toft, J., and Cooper, K.M., 2017, Shallow melting of MORB-like mantle under hot continental lithosphere, central Anatolia: Geosphere, v. 18, p. 1866–1888.

Richards, J.P., 2003, Tectono-magmatic precursors for porphyry Cu-(Mo-Au) deposit formation: Economic Geology, v. 98, p. 1515–1533.

——2009, Postsubduction porphyry Cu-Au and epithermal Au deposits: Products of remelting of subduction-modified lithosphere: Geology, v. 37, p. 247–250.

——2011, Magmatic to hydrothermal metal fluxes in convergent and collided margins: Ore Geology Reviews, v. 40, p. 1–26.

——2015, Tectonic, magmatic, and metallogenic evolution of the Tethyan orogen: From subduction to collision: Ore Geology Reviews, v. 70, p. 323–345.

Robertson, A.H.F., Parlak, O., Rızaoğlu, T., Ünlügenç, Ü., İnan, N., Taşlı, K., and Ustaömer, T., 2007, Tectonic evolution of the south Tethyan ocean: Evidence from the eastern Taurus Mountains (Elazığ region, SE Turkey): Geological Society of London Special Publication 272, p. 231–270.

Sánchez, M.G., McClay, K.R., King, A.R., and Wijbrams, J.R., 2016, Cenozoic crustal extension and its relationship to porphyry Cu-Au-(Mo) and epithermal Au-(Ag) mineralization in the Biga peninsula, northwestern Turkey: Society of Economic Geologists Special Publication 19, p. 113–156.

Schildgen, T.F., Cosentino, D., and Bookhagen, B., 2012, Multi-phased uplift of the southern margin of the central Anatolian Plateau, Turkey: A record of tectonic and upper mantle processes: Earth and Planetary Science Letters, v. 317-318, p. 85–95.

Shinohara, H., and Hedenquist, J.W., 1997, Constraints on magma degassing beneath the Far Southeast porphyry Cu-Au deposit, Philippines: Journal of Petrology, v. 38, p. 1741–1752.

Sillitoe, R.H., 2000, Gold-rich porphyry deposits: Descriptive and genetic models and their role in exploration and discovery: Reviews in Economic Geology, v. 13, p. 315–345.

——2005, Supergene oxidized and enriched porphyry copper and related deposits: Economic Geology 100th Anniversary Volume, p. 723–768.

——2010, Porphyry copper systems: Economic Geology, v. 105, p. 3–41.

Sönmez, Ş.U., and Kuşcu, İ., 2020, Geology, geochemistry, geochronology and genesis of the late Miocene porphyry Cu-Au-Mo mineralization at Afyon-Sandıklı (AS) prospect, western Anatolia, Turkey: Ore Geology Reviews, v. 121, 103506.

Steven, T.A., and Ratté, J.C., 1960, Geology of ore deposits of the Summitville district, San Juan Mountains, Colorado: U.S. Geological Survey Professional Paper 343, 70 p.

Stoffregen, R.E., 1987, Genesis of acid-sulfate alteration and Au-Cu-Ag mineralization at Summitville, Colorado: Economic Geology, v. 82, p. 1575–1591.

Toprak, V., and Göncüoğlu, M.C., 1993, Tectonic control on the development of the Neogene-Quaternary central Anatolian Volcanic Province, Turkey: Geological Journal, v. 28, p. 357–369.

Tosdal, R.M., and Richards, J.P., 2001, Magmatic and structural controls on the development of porphyry Cu ± Mo ± Au deposits: Reviews in Economic Geology, v. 14, p. 157–180.

Türkecan, A., Akçay, A.E., Satır, M., Dönmez, M., and Ercan, T., 2003, Melendiz Dağları (Niğde) volkanizması [ext. abs.]: Geological Congress of Turkey, 56th, Ankara, Turkey, Extended Abstracts, p. 16–17 (in Turkish with English abst.).

Ulrich, T., and Heinrich, C.A., 2002, Geology and alteration geochemistry of the porphyry Cu-Au deposit at Bajo de la Alumbrera, Argentina: Economic Geology, v. 97, p. 1865–1888.

Wilkinson, J.J., 2013, Triggers for the formation of porphyry ore deposits in magmatic arcs: Nature Geoscience, v. 6, p. 917–925.

Yiğit, Ö., 2009, Mineral deposits of Turkey in relation to Tethyan metallogeny: Implications for future mineral exploration: Economic Geology, v. 104, p. 19–51.

——2012, A prospective sector in the Tethyan metallogenic belt: Geology and geochronology of mineral deposits in the Biga Peninsula, NW Turkey: Ore Geology Reviews v. 46, p. 118–148.

Yıldız, B., 2013, The Miocene-Pliocene metallogenic belt in between Tauride and Anatolide blocks [abs.]: Geological Congress of Turkey, 66th, Ankara, April 1–5, 2013, Abstracts, p. 414–415.

Yıldız, B., Sillitoe, R.H., Foster, R., Hall, D., and Stallman, M., 2016, Discovery of the Öksüt million-ounce high sulfidation gold deposit: Society of Economic Geologists, Tethyan Tectonics and Metallogeny Conference, September 25–28, 2016, Çeşme, Turkey, Proceedings, 1 p.

——2017, Öksüt: A high-sulphidation epithermal gold discovery in Turkey: NewGenGold 2017 Conference Proceedings, West Perth, Paydirt Media Pty Ltd., p. 273–287.

Emrecan Yurdakul is an exploration geologist for Centerra Gold Inc., mainly looking for gold-copper mineralization within the Turkish part of the Neotethyan belt. Emrecan earned a bachelor's degree from the Middle East Technical University, Turkey, and is currently undertaking his master's degree program at the same institution. His graduate research focuses on understanding the formation of the Öksüt high-sulfidation gold-copper deposit.